

Energy Stable Nodal Discontinuous Galerkin Methods for Nonlinear Maxwell's Equations in Multi-dimensions

Maohui Lyu¹ · Vrushali A. Bokil² · Yingda Cheng³ · Fengyan Li⁴

Received: 8 June 2021 / Revised: 25 August 2021 / Accepted: 5 September 2021 © The Author(s), under exclusive licence to Springer Science+Business Media, LLC, part of Springer Nature 2021

Abstract

In this work, we extend the energy stable discontinuous Galerkin (DG) schemes proposed in Bokil et al. (J Comput Phys 350:420–452, 2017), for the time domain Maxwell's equations augmented with a class of nonlinear constitutive polarization laws, to higher dimensions. The nontrivial discrete temporal treatment of the nonlinearity in the ordinary differential equations that encode the Kerr and Raman effects (Bokil et al. 2017), is first generalized to higher spatial dimensions. To further improve the computational efficiency in dealing with the nonlinearity, we apply nodal DG methods in space. Energy stability is proved for the semi-discrete in time and in space schemes as well as for the fully-discrete schemes. Under some assumptions on the strength of nonlinearity, error estimates are established for the semi-discrete in space methods, and, in particular, optimal accuracy is achieved for the methods on Cartesian meshes with Q^k -type elements and alternating fluxes. Attention is paid to the role of the nodal form of the DG discretizations in the analysis. We numerically

Maohui Lyu: Research is supported by China Postdoctoral Science Foundation 2020TQ0344, and NSFC Grants 11871139 and 12101597. Vrushali A. Bokil: Research is supported by NSF Grants DMS-1720116 and DMS-2012882. Yingda Cheng: Research is supported by NSF Grants DMS-1453661 and DMS-2011838. Fengyan Li: Research is supported by NSF Grants DMS-1719942 and DMS-1913072.

> Maohui Lyu mlyu@lsec.cc.ac.cn

Vrushali A. Bokil bokilv@math.oregonstate.edu

Published online: 11 October 2021

Yingda Cheng ycheng@msu.edu

- State Key Laboratory of Scientific and Engineering Computing (LSEC), Academy of Mathematics and System Sciences, Chinese Academy of Sciences, Beijing 100190, China
- Department of Mathematics, College of Science, Oregon State University, Corvallis, OR 97331, USA
- Department of Mathematics, Department of Computational Mathematics, Science and Engineering, Michigan State University, East Lansing, MI 48824, USA
- Department of Mathematical Sciences, Rensselaer Polytechnic Institute, Troy, NY 12180, USA



validate the accuracy, energy stability, and computational efficiency of the proposed schemes using manufactured solutions. We further illustrate the performance of the methods through physically relevant experiments involving spatial soliton propagation and airhole scattering in realistic glasses.

Keywords Maxwell's equations · Kerr and Raman nonlinear effects · Linear Lorentz · Nodal discontinuous Galerkin methods · Energy stable · High dimensions

1 Introduction

When light propagates in an optical medium, it interacts with the medium. The response of the medium to the incident light can be linear or nonlinear, and can have varying timescales. The nonlinear responses play a significant role especially when the intensity of incident wave is strong, and they contribute to many extraordinary optical phenomena, such as high order harmonic generation and four wave mixing [6]. It is well known that the governing equations for these optical phenomena are the classical Maxwell's partial differential equations (PDEs), either in microscopic version or in macroscopic form [18,21]. The microscopic Maxwell's equations focus on the dynamics of individual charged particles under the influence of electromagetic fields. On the other hand, macroscopic Maxwell's equations characterize the medium's response through constitutive relations modeling the dynamical evolution of the macroscopic polarization, defined as the average dipole moment per unit volume, forced by the electromagnetic field intensity. In magnetic materials, the model needs to account for the evolution of the macroscopic magnetization.

In this paper, we consider the following macroscopic Maxwell's equations on $\Omega \times [0, T]$,

$$\mu_0 \partial_t \mathbf{H} + \nabla \times \mathbf{E} = \mathbf{0},\tag{1a}$$

$$\partial_t \mathbf{D} - \nabla \times \mathbf{H} = \mathbf{0},\tag{1b}$$

$$\mathbf{D} = \epsilon_0 \Big(\epsilon_\infty \mathbf{E} + \mathbf{P} + a(1 - \theta) |\mathbf{E}|^2 \mathbf{E} + a\theta Q \mathbf{E} \Big), \tag{1c}$$

$$\partial_t \boldsymbol{P} = \boldsymbol{J},\tag{1d}$$

$$\partial_t \mathbf{J} + \gamma \mathbf{J} + \omega_0^2 \mathbf{P} = \omega_p^2 \mathbf{E},\tag{1e}$$

$$\partial_t Q = \sigma,$$
 (1f)

$$\partial_t \sigma + \gamma_v \sigma + \omega_v^2 Q = \omega_v^2 |E|^2, \tag{1g}$$

with the initial conditions and suitable boundary conditions. Here $\Omega = [x_a, x_b] \times [y_a, y_b] \times [z_a, z_b] \subset \mathbb{R}^d$ (d=2,3) is the spatial domain, and [0,T] is the time period in consideration. In this model, apart from the instantaneous linear response $\epsilon_0 \epsilon_\infty E$, a retarded or delayed response, $\epsilon_0 P$, modeled as a linear dispersive Lorentz effect governed by the ordinary differential equations (ODEs) (1d)–(1e) is included. In addition, this model also takes into account the third order instantaneous nonlinear Kerr effect $\epsilon_0 a(1-\theta)|E|^2E$ and the nonlinear dispersive Raman effect $\epsilon_0 a\theta QE$. The constants a and θ parameterize the strength and relative strength of these two nonlinearities. The dynamics of Q is described by the nonlinear ODEs (1f)–(1g). We refer the readers to [3,13] for more detailed description of this model.



For the system above, if we define the energy $\mathcal{E} = \mathcal{E}(t)$ as

$$\mathcal{E} = \int_{\Omega} \frac{\mu_0}{2} |\mathbf{H}|^2 + \frac{\epsilon_0 \epsilon_{\infty}}{2} |\mathbf{E}|^2 + \frac{\epsilon_0}{2\omega_p^2} |\mathbf{J}|^2 + \frac{\epsilon_0 \omega_0^2}{2\omega_p^2} |\mathbf{P}|^2 + \frac{\epsilon_0 a\theta}{4\omega_v^2} \sigma^2 + \frac{\epsilon_0 a\theta}{2} Q |\mathbf{E}|^2 + \frac{3\epsilon_0 a(1-\theta)}{4} |\mathbf{E}|^4 + \frac{\epsilon_0 a\theta}{4} Q^2 d\Omega,$$
 (2)

then, under periodic boundary conditions in space, the energy satisfies the identity [3]

$$\frac{d}{dt}\mathcal{E} = -\frac{\epsilon_0 \gamma}{\omega_p^2} \int_{\Omega} |\boldsymbol{J}|^2 d\Omega - \frac{\epsilon_0 a \theta \gamma_v}{2\omega_v^2} \int_{\Omega} \sigma^2 d\Omega \le 0. \tag{3}$$

We further assume $\theta \in [0, \frac{3}{4}]$, then

$$\frac{\epsilon_0 a \theta}{2} Q |\mathbf{E}|^2 + \frac{3\epsilon_0 a (1-\theta)}{4} |\mathbf{E}|^4 + \frac{\epsilon_0 a \theta}{4} Q^2 = \frac{\epsilon_0 a \theta}{4} \left(|\mathbf{E}|^2 + Q \right)^2 + \frac{\epsilon_0 a (3-4\theta)}{4} |\mathbf{E}|^4 \ge 0,$$

and therefore $\mathcal{E}(t) \geq 0$. This suggests that, on the continuous level, the system (1) is energy stable.

The goal of this work is to design energy stable numerical schemes that can preserve the stability relation (3) at the discrete level. For wave propagation problems, energy preserving schemes are always favorable since they are able to maintain the shape and phase of the waves accurately after long time simulations [23]. In [3] and [4], energy stable discontinuous Galerkin (DG) schemes, and finite difference time domain (FDTD) schemes, respectively, were developed for the model (1) in one dimension (1D), which are of second order temporal accuracy and have arbitrary order spatial accuracy. To the best of our knowledge, there are no numerical methods with provable energy stability available for the Maxwell's equations (1) involving both nonlinear Kerr and Raman effects along with the linear Lorentz dispersion in higher dimensions.

In [19], a FDTD method was developed for the transverse magnetic (TM) mode of Maxwell's equations in nonlinear Kerr type media only ($\theta = 0$). For this 2D model, there is no essential new difficulty to handle the nonlinearity beyond what was discussed in [3], and the same 1D treatment as in [3] was adopted directly. Recently, in [1], an energy stable time domain finite element method was developed for the 3D Maxwell's equations with the nonlinear Kerr effect only ($\theta = 0$), and without the linear Lorentz and nonlinear Raman dispersive effects. Moreover, theoretical investigation of the developed scheme is lacking.

In this paper, we extend the schemes proposed in [3] for the 1D version of model (1) to higher spatial dimensions. The main challenge in the design of provable energy stable schemes for the nonlinear Maxwell's equations lies in the time discretizations. In [3], based on a novel strategy in dealing with nonlinear terms, the authors proposed semi-explicit leapfrog and fully-implicit trapezoidal type DG schemes for the 1D model. In this work, we extend the results to higher dimensions by introducing an auxiliary vector to discretize the temporal difference of the nonlinear cubic term for the Kerr effect in the constitutive relation. To achieve provable energy stable time discretizations in high dimensions, one needs to take into account the vector nature of the electric field, whose components are now coupled through a nonlinear relationship.

As for spatial discretizations, there are many numerical approaches available for the Maxwell's equations. Among them, FDTD and generalized mimetic finite difference methods [5], finite element methods and DG methods have drawn a lot of attention in the scientific



community in recent decades, especially for linear constitutive laws in Maxwell's equations. For Maxwell's equations with nonlinear constitutive laws, to name a few, in [14,15], a GVADE FDTD method was proposed and investigated for simulations in 2D realistic glasses characterized by linear Lorentz, nonlinear Kerr and Raman effects. In [2], high order energy stable FDTD methods of summation-by-parts type were designed for 2D Maxwell-Duffing models. Mixed finite element methods were developed for the nonlinear Kerr model in [1] and for the relaxed Kerr-Debye model in [12]. By regarding the system as nonlinear hyperbolic conservation laws, DG methods were examined for the nonlinear Kerr model in [11]. Asymptotic-preserving and positivity-preserving DG methods were proposed and analyzed for the 1D relaxed Kerr-Debye model in [17] and for this relaxed model with an additional linear Lorentz dispersion effect in [22].

In this work, we rely on DG methods as our spatial discretizations for the nonlinear Maxwell model under consideration. For DG schemes, the choice of numerical fluxes is the key to the stability, accuracy and computational efficiency of the method. In [3], energy stable DG schemes with central, alternating and upwind numerical fluxes were designed for the 1D model. The authors recommend the leap-frog DG schemes with alternating fluxes, due to their optimal accuracy and the local nature of nonlinear algebraic solvers. The extensions of the schemes to higher dimensions require more careful consideration. For d > 1, it has been reported that the DG methods with alternating numerical fluxes suffer from sub-optimal accuracy when P^k -type elements are used [20]. In this paper, we employ Q^k -type elements on Cartesian meshes to attain optimal order of accuracy. Note that the O^k -type DG space is larger than the P^k -type one. This makes the methods relatively more expensive. To boost the efficiency, we adopt nodal DG formulations [16], which, with some numerical integration built-in to the definition of the methods, provide a natural and efficient way to handle the nonlinearity [10,22]. Compared with the modal formulation of the DG methods (previously adopted in [3] for 1D), the nodal form allows the element-wise nonlinear algebraic systems to be further decoupled into several smaller ones (see Remark 3, and numerical comparison in Sect. 3.1). To better convey how the temporal discretizations and the nodal-form of the spatial discretizations contribute to the energy stability of the numerical methods, we establish the energy stability for the semi-discrete in time and the semi-discrete in space schemes separately, before presenting a similar result for fully-discrete schemes. For the semi-discrete in space nodal DG schemes, we also carry out error estimates under some assumptions on the strength of the nonlinearity that is considered in this paper. In particular, we confirm the optimal accuracy of the schemes with Q^k elements and alternating numerical fluxes. Although the presentation and the analysis related to the spatial discretization are given for the 2D transverse electric (TE) mode of Maxwell's equations in this paper, the extension to the 3D model is straightforward. We want to point out that there is some difference in analysis for the nodal form of the DG spatial discretizations here compared with that for the modal form in [3].

The remainder of the paper is organized as follows. In Sect. 2, we formulate the proposed numerical schemes. Particularly, in Sect. 2.1, by a similar strategy introduced in [3] to handle the nonlinearity, we extend the leap-frog type time discretization to the 3D nonlinear Maxwell's equations with provable energy stability. In Sect. 2.2, the nodal DG schemes are formulated for the 2D nonlinear Maxwell's equations in the TE mode. Energy stability and error estimates are presented for the semi-discrete in space schemes with the Q^k -type elements. In Sect. 2.3, we present the fully discrete schemes and their energy stability property. In Sect. 3, we numerically demonstrate the accuracy, energy stability, as well as the computational efficiency of the proposed schemes by several 2D experiments. Our schemes are



further applied to simulate the spatial soliton propagation and airhole scattering in realistic glasses. Finally, conclusions are made in Sect. 4.

2 Numerical Schemes

In this section, we will introduce a family of numerical schemes for the Maxwell's equations (1) in nonlinear media. We will start with the semi-discrete in time method in Sect. 2.1, then present a class of semi-discrete in space methods in Sect. 2.2, followed by the fully-discrete schemes in Sect. 2.3. For both semi-discrete and fully-discrete methods, energy stability will be established. Error estimates will also be proved for the semi-discrete in space schemes. Periodic boundary conditions are assumed in space throughout this section, while other boundary conditions are considered for numerical experiments in Sect. 3.

2.1 Semi-discrete in Time Method

In [3], based on a novel strategy for dealing with nonlinear terms, the authors proposed semi-explicit leap-frog and fully implicit trapezoidal type DG schemes for the 1D version of model (1). Both types of schemes enjoy provable discrete energy stable property. Moreover, a fully discrete energy stability analysis suggests that the trapezoidal DG schemes are unconditionally stable, while the leap-frog DG schemes are optimally stable in the sense that the same CFL condition for the numerical schemes applied to Maxwell's equations in the simple linear media with $D = \epsilon_0 \epsilon_\infty E$ in (1c) is valid for the schemes for Maxwell's equations in the nonlinear media considered in this paper. For the trapezoidal DG schemes, since both the PDE part and the ODE part use implicit discretizations, at each time step, one has to solve a global nonlinear system. Therefore, in this work, we only consider the leap-frog scheme for discretization of the PDE part of the model, and this only involves a local nonlinear solver. The extension to fully implicit trapezoidal schemes can be constructed in an analogous manner and is omitted for the reason of efficiency. In particular, we propose the following semi-discrete in time scheme that uses the leap-frog method for the PDE part and the trapezoidal method for the ODE part of the equations (1), combined with special treatments for nonlinear terms.

Given H^n , E^n , D^n , J^n , P^n , σ^n and Q^n at time $t = t^n$, we find H^{n+1} , E^{n+1} , D^{n+1} , J^{n+1} , P^{n+1} , σ^{n+1} and Q^{n+1} at time $t^{n+1} = t^n + \Delta t$, satisfying

$$\mu_0 \frac{\boldsymbol{H}^{n+1/2} - \boldsymbol{H}^n}{\Delta t/2} = -\nabla \times \boldsymbol{E}^n, \tag{4a}$$

$$\frac{\boldsymbol{D}^{n+1} - \boldsymbol{D}^n}{\Delta t} = \nabla \times \boldsymbol{H}^{n+1/2},\tag{4b}$$

$$\boldsymbol{D}^{n+1} = \epsilon_0 \Big(\epsilon_\infty \boldsymbol{E}^{n+1} + a(1-\theta) \boldsymbol{Y}^{n+1} + \boldsymbol{P}^{n+1} + a\theta \, \boldsymbol{Q}^{n+1} \boldsymbol{E}^{n+1} \Big),$$

$$Y^{n+1} - Y^n = (|E^{n+1}|^2 + |E^n|^2 - E^{n+1} \cdot E^n)(E^{n+1} - E^n)$$
 (4c)

$$+\frac{1}{2}\Big((E^{n+1}+E^n)\cdot(E^{n+1}-E^n)\Big)(E^{n+1}+E^n),\tag{4d}$$

$$\frac{P^{n+1} - P^n}{\Delta t} = \frac{J^{n+1} + J^n}{2},\tag{4e}$$

$$\frac{J^{n+1} - J^n}{\Delta t} + \gamma \frac{J^{n+1} + J^n}{2} + \omega_0^2 \frac{P^{n+1} + P^n}{2} = \omega_p^2 \frac{E^{n+1} + E^n}{2},$$
 (4f)

$$\frac{Q^{n+1} - Q^n}{\Delta t} = \frac{\sigma^{n+1} + \sigma^n}{2},\tag{4g}$$

$$\frac{\sigma^{n+1} - \sigma^n}{\Delta t} + \gamma_v \frac{\sigma^{n+1} + \sigma^n}{2} + \omega_v^2 \frac{Q^{n+1} + Q^n}{2} = \omega_v^2 E^{n+1} \cdot E^n, \tag{4h}$$

$$\mu_0 \frac{\mathbf{H}^{n+1} - \mathbf{H}^{n+1/2}}{\Delta t/2} = -\nabla \times \mathbf{E}^{n+1}.$$
 (4i)

Leap-frog and trapezoidal methods are chosen for their symplectic nature. Nonlinear Kerr and Raman terms are further discretized in such a way that an energy relation similar to that at the continuous level will hold. More specifically, to discretize the Kerr term, we introduce an auxiliary vector $Y = |E|^2 E$ as in [3] for the one dimensional model, and consider its temporal dynamics written in the following way

$$\partial_t Y = \partial_t \left(|\mathbf{E}|^2 \mathbf{E} \right) = \left(3|\mathbf{E}|^2 - 2|\mathbf{E}|^2 \right) \partial_t \mathbf{E} + 2\left(\mathbf{E} \cdot \partial_t \mathbf{E} \right) \mathbf{E}. \tag{5}$$

We then apply a second order discretization to (5),

$$\mathbf{Y}^{n+1} - \mathbf{Y}^{n} = \left(3\frac{|\mathbf{E}^{n+1}|^{2} + |\mathbf{E}^{n}|^{2}}{2} - 2\left|\frac{\mathbf{E}^{n+1} + \mathbf{E}^{n}}{2}\right|^{2}\right) (\mathbf{E}^{n+1} - \mathbf{E}^{n}) + 2\left(\frac{\mathbf{E}^{n+1} + \mathbf{E}^{n}}{2} \cdot (\mathbf{E}^{n+1} - \mathbf{E}^{n})\right) \frac{\mathbf{E}^{n+1} + \mathbf{E}^{n}}{2},$$
(6)

which yields (4d). For Raman term $|E|^2$, a second order discretization $E^{n+1} \cdot E^n$ is employed. With all these ingredients, the proposed method has the energy stability property as presented in Theorem 1 below. Similar strategies for energy stable semi-discrete in time schemes have been employed in [3] for models in one dimension and [1] for models in three dimensions with the Kerr effect.

Theorem 1 (Semi-discrete in time energy stability) *Under the assumption of periodic bound*ary conditions, the semi-discrete in time scheme (4) satisfies

$$\mathcal{E}^{n+1} - \mathcal{E}^{n} = -\frac{\epsilon_{0}\gamma \Delta t}{4\omega_{p}^{2}} \int_{\Omega} \left| \boldsymbol{J}^{n+1} + \boldsymbol{J}^{n} \right|^{2} d\Omega - \frac{\epsilon_{0}a\theta\gamma_{v}\Delta t}{8\omega_{v}^{2}} \int_{\Omega} \left(\sigma^{n+1} + \sigma^{n} \right)^{2} d\Omega \le 0$$
(7)

with the discrete energy defined as

$$\mathcal{E}^{n} = \int_{\Omega} \frac{\mu_{0}}{2} \boldsymbol{H}^{n+1/2} \cdot \boldsymbol{H}^{n-1/2} + \frac{\epsilon_{0} \epsilon_{\infty}}{2} \left| \boldsymbol{E}^{n} \right|^{2} + \frac{\epsilon_{0}}{2\omega_{p}^{2}} \left| \boldsymbol{J}^{n} \right|^{2} + \frac{\epsilon_{0} \omega_{0}^{2}}{2\omega_{p}^{2}} \left| \boldsymbol{P}^{n} \right|^{2} + \frac{\epsilon_{0} a \theta}{4\omega_{v}^{2}} (\sigma^{n})^{2} + \frac{\epsilon_{0} a \theta}{2} Q^{n} \left| \boldsymbol{E}^{n} \right|^{2} + \frac{3\epsilon_{0} a (1 - \theta)}{4} \left| \boldsymbol{E}^{n} \right|^{4} + \frac{\epsilon_{0} a \theta}{4} (Q^{n})^{2} d\Omega.$$
(8)

Proof Apply two time steps to (4a) and (4i), we have

$$\mu_0 \frac{H^{n+3/2} - H^{n-1/2}}{\Delta t} = -\nabla \times (E^{n+1} + E^n). \tag{9}$$

Multiply $E^{n+1} + E^n$ to (4b), multiply $H^{n+1/2}$ to (9), integrate over Ω and sum them up, and use periodic boundary conditions, we obtain



$$\mu_0 \int_{\Omega} \mathbf{H}^{n+3/2} \cdot \mathbf{H}^{n+1/2} - \mathbf{H}^{n+1/2} \cdot \mathbf{H}^{n-1/2} d\Omega + \int_{\Omega} (\mathbf{D}^{n+1} - \mathbf{D}^n) \cdot (\mathbf{E}^{n+1} + \mathbf{E}^n) d\Omega = 0.$$
(10)

From (4c), one has

$$(\mathbf{D}^{n+1} - \mathbf{D}^{n}) \cdot (\mathbf{E}^{n+1} + \mathbf{E}^{n})$$

$$= \epsilon_{0} \epsilon_{\infty} \left(|\mathbf{E}^{n+1}|^{2} - |\mathbf{E}^{n}|^{2} \right) + \epsilon_{0} a (1 - \theta) (\mathbf{Y}^{n+1} - \mathbf{Y}^{n}) \cdot (\mathbf{E}^{n+1} + \mathbf{E}^{n})$$

$$+ \epsilon_{0} (\mathbf{P}^{n+1} - \mathbf{P}^{n}) \cdot (\mathbf{E}^{n+1} + \mathbf{E}^{n}) + \epsilon_{0} a \theta (\mathbf{Q}^{n+1} \mathbf{E}^{n+1} - \mathbf{Q}^{n} \mathbf{E}^{n}) \cdot (\mathbf{E}^{n+1} + \mathbf{E}^{n}).$$
(11)

For the nonlinear Kerr term in (11), with the proposed treatment in (4d), we get

$$(\mathbf{Y}^{n+1} - \mathbf{Y}^n) \cdot (\mathbf{E}^{n+1} + \mathbf{E}^n)$$

$$= \left(|\mathbf{E}^{n+1}|^2 + |\mathbf{E}^n|^2 - \mathbf{E}^{n+1} \cdot \mathbf{E}^n + \frac{1}{2} |\mathbf{E}^{n+1} + \mathbf{E}^n|^2 \right) \left(|\mathbf{E}^{n+1}|^2 - |\mathbf{E}^n|^2 \right)$$

$$= \frac{3}{2} \left| \mathbf{E}^{n+1} \right|^4 - \frac{3}{2} \left| \mathbf{E}^n \right|^4.$$
(13)

For the Lorentz term in (11), using (4e) and (4f), we have

$$(\mathbf{P}^{n+1} - \mathbf{P}^{n}) \cdot (\mathbf{E}^{n+1} + \mathbf{E}^{n})$$

$$= \frac{2}{\omega_{p}^{2}} (\mathbf{P}^{n+1} - \mathbf{P}^{n}) \cdot \left(\frac{\mathbf{J}^{n+1} - \mathbf{J}^{n}}{\Delta t} + \frac{\gamma}{2} (\mathbf{J}^{n+1} + \mathbf{J}^{n}) + \frac{\omega_{0}^{2}}{2} (\mathbf{P}^{n+1} + \mathbf{P}^{n}) \right)$$

$$= \frac{1}{\omega_{p}^{2}} |\mathbf{J}^{n+1}|^{2} - \frac{1}{\omega_{p}^{2}} |\mathbf{J}^{n}|^{2} + \frac{\gamma \Delta t}{2\omega_{p}^{2}} |\mathbf{J}^{n+1} + \mathbf{J}^{n}|^{2} + \frac{\omega_{0}^{2}}{\omega_{p}^{2}} |\mathbf{P}^{n+1}|^{2} - \frac{\omega_{0}^{2}}{\omega_{p}^{2}} |\mathbf{P}^{n}|^{2}. \quad (14)$$

Finally for the nonlinear Raman term in (11), we have

$$(Q^{n+1}E^{n+1} - Q^nE^n) \cdot (E^{n+1} + E^n)$$

$$= Q^{n+1}|E^{n+1}|^2 - Q^n|E^n|^2 + (Q^{n+1} - Q^n)(E^{n+1} \cdot E^n), \tag{15}$$

where by using (4g) and (4h),

$$(Q^{n+1} - Q^n)(E^{n+1} \cdot E^n)$$

$$= \frac{1}{\omega_v^2} (Q^{n+1} - Q^n) \left(\frac{\sigma^{n+1} - \sigma^n}{\Delta t} + \frac{\gamma_v}{2} (\sigma^{n+1} + \sigma^n) + \frac{\omega_v^2}{2} (Q^{n+1} + Q^n) \right)$$

$$= \frac{1}{2\omega_v^2} (\sigma^{n+1})^2 - \frac{1}{2\omega_v^2} (\sigma^n)^2 + \frac{\gamma_v \Delta t}{4\omega_v^2} \left(\sigma^{n+1} + \sigma^n \right)^2 + \frac{1}{2} (Q^{n+1})^2 - \frac{1}{2} (Q^n)^2.$$
 (16)

Combining (10)–(16), we reach the semi-discrete in time energy stability (7). \Box

2.2 Semi-discretization in Space: Nodal Discontinuous Galerkin Methods

In this section, we will formulate a class of nodal discontinuous Galerkin (DG) methods in space for the Maxwell's equations (1). The nodal version of DG discretizations is chosen in this work for its computational efficiency in dealing with nonlinear terms, while preserving the energy relation. For simplicity, we present the method only for the 2D transverse electric



(TE) mode. Extension to the full 3D model is straightforward. Thus, we consider the 2D system of equations

$$\mu_0 \partial_t H_z + \partial_x E_v - \partial_v E_x = 0, \tag{17a}$$

$$\partial_t D_x - \partial_y H_z = 0, (17b)$$

$$\partial_t D_v + \partial_x H_z = 0, \tag{17c}$$

$$\mathbf{D} = \epsilon_0 \Big(\epsilon_\infty \mathbf{E} + \mathbf{P} + a(1 - \theta) |\mathbf{E}|^2 \mathbf{E} + a\theta Q \mathbf{E} \Big), \tag{17d}$$

$$\partial_t \mathbf{P} = \mathbf{J},\tag{17e}$$

$$\partial_t \mathbf{J} + \gamma \mathbf{J} + \omega_0^2 \mathbf{P} = \omega_p^2 \mathbf{E},\tag{17f}$$

$$\partial_t Q = \sigma, \tag{17g}$$

$$\partial_t \sigma + \gamma_v \sigma + \omega_v^2 Q = \omega_v^2 |E|^2. \tag{17h}$$

Here, all vector fields have two components polarized in the x - y plane, $\mathbf{D} = (D_x, D_y)$, $E = (E_x, E_y), P = (P_x, P_y), \text{ and } J = (J_x, J_y).$

Mesh, discrete space, and interpolation operator. Assume the computational domain is $\Omega = [x_a, x_b] \times [y_a, y_b]$. Let $\mathcal{T}_{xh} : x_a = x_{\frac{1}{2}} < x_{\frac{3}{2}} < \dots < x_{N_x + \frac{1}{2}} = x_b$ be a partition of $[x_a, x_b]$, and $\mathcal{T}_{yh}: y_a = y_{\frac{1}{2}} < y_{\frac{3}{2}} < \dots < y_{N_v + \frac{1}{2}} = y_b$ be a partition of $[y_a, y_b]$, then

$$\mathcal{T}_h = \mathcal{T}_{xh} \times \mathcal{T}_{yh} = \left\{ K_{ij} = I_i \times J_j, I_i = [x_{i-\frac{1}{2}}, x_{i+\frac{1}{2}}], J_j = [y_{j-\frac{1}{2}}, y_{j+\frac{1}{2}}], \forall i, j \right\}$$

forms a partition or a mesh of Ω . For a typical cell K_{ij} , we denote the cell center as (x_i, y_j) $\left(\frac{1}{2}(x_{i+\frac{1}{2}} + x_{x-\frac{1}{2}}), \frac{1}{2}(y_{j+\frac{1}{2}} + y_{j-\frac{1}{2}})\right)$, and the grid size as $\Delta x_i = x_{i+\frac{1}{2}} - x_{i-\frac{1}{2}}$, $\Delta y_j = x_{i+\frac{1}{2}} - x_{i+\frac{1}{2}} - x_{i+\frac{1}{2}}$ $y_{j+\frac{1}{2}} - y_{j-\frac{1}{2}}$ in the x and y directions, respectively. Let $h = \max_{i} (\Delta x_i, \Delta y_j)$. We further assume the mesh is quasi-uniform, namely, there exists a constant δ such that $\frac{h}{\min(\Delta x_i, \Delta y_j)} < \delta$ as the mesh is refined.

Associated with the mesh, we introduce a discrete space of Q^k -type,

$$V_h^k = \left\{ v \in L^2(\Omega) : v|_{K_{ij}} \in Q^k(K_{ij}), \ \forall i, j \right\},\tag{18}$$

where $Q^k(K_{ij})$ consists of polynomials with degree up to k in each variable on K_{ij} . Without confusion, V_h^k is also used to represent its vector version in this work. For any function $v \in V_h^k$, we write

$$v(x_{i+\frac{1}{2}}^{\pm}, y) = \lim_{\epsilon \to 0\pm} v(x_{i+\frac{1}{2}} + \epsilon, y), \quad v(x, y_{j+\frac{1}{2}}^{\pm}) = \lim_{\epsilon \to 0\pm} v(x, y_{j+\frac{1}{2}} + \epsilon).$$

We further write the average and jump of v(x, y) at cell interface $x = x_{i+\frac{1}{2}}$ as

$$\{v\}_{x_{i+\frac{1}{2}}} = \frac{1}{2} \Big(v(x_{i+\frac{1}{2}}^+, y) + v(x_{i+\frac{1}{2}}^-, y) \Big), \quad [v]_{x_{i+\frac{1}{2}}} = v(x_{i+\frac{1}{2}}^+, y) - v(x_{i+\frac{1}{2}}^-, y),$$

respectively. Similarly, the average and jump of $v(x, y_{j+\frac{1}{2}})$ at cell interface $y = y_{j+\frac{1}{2}}$ are defined as

$$\{v\}_{y_{j+\frac{1}{2}}} = \frac{1}{2} \left(v(x, y_{j+\frac{1}{2}}^+) + v(x, y_{j+\frac{1}{2}}^-) \right), \quad [v]_{y_{j+\frac{1}{2}}} = v(x, y_{j+\frac{1}{2}}^+) - v(x, y_{j+\frac{1}{2}}^-).$$

For nodal DG formulation, we introduce the Gauss-Legendre quadrature points as $\{\xi_m\}_{m=0}^k$ on [-1, 1] with positive weights $\{\widehat{w}_m\}_{m=0}^k$, satisfying $\sum_{m=0}^k \widehat{w}_m = 2$. We let $\{l_n(\xi)\}_{n=0}^k$ be



the Lagrange basis of $P^k([-1, 1])$, the space of polynomials of degree up to k on [-1, 1], satisfying $l_n(\xi_m) = \delta_{nm}$. Here δ_{nm} is the Kronecker delta. Define

$$\phi_{mn}^{ij}(x,y) = l_m(\frac{x-x_i}{\Delta x_i/2})l_n(\frac{y-y_j}{\Delta y_j/2}),$$

then $\left\{\phi_{mn}^{ij}(x,y)\right\}_{m,n=0}^{k}$ forms an orthogonal basis for $V_h^k(K_{ij}) = Q^k(K_{ij})$. We also write $x_{im} = x_i + \frac{\Delta x_i}{2} \xi_m$ and $y_{jn} = y_j + \frac{\Delta y_j}{2} \xi_n$.

On any given element K_{ij} , we define a local interpolation operator $\mathcal{I}_h^{ij}:C(K_{ij})\mapsto Q^k(K_{ij})$ that satisfies $\left(\mathcal{I}_h^{ij}f\right)(x_{im},y_{jn})=f(x_{im},y_{jn}), \forall m,n=0,\cdots,k$. It can be expressed analytically as

$$\left(\mathcal{I}_{h}^{ij}f\right)(x,y) = \sum_{m,n=0}^{k} f(x_{im}, y_{jn})\phi_{mn}^{ij}(x,y). \tag{19}$$

Subsequently, we can define a global interpolation operator $\mathcal{I}_h: W_h(\Omega) \mapsto V_h^k$, with $\mathcal{I}_h|_{K_{ij}} = \mathcal{I}_h^{ij}$. Here $W_h(\Omega) = \left\{ f \in L^2(\Omega), \, f|_{K_{ij}} \in C(K_{ij}), \, \forall i, j \right\}$. The interpolation operator \mathcal{I}_h has the following properties.

Lemma 1 For any $f, g \in W_h(\Omega)$, there hold

$$\int_{\Omega} \mathcal{I}_h(fg) d\Omega = \int_{\Omega} \mathcal{I}_h(f) \mathcal{I}_h(g) d\Omega, \tag{20}$$

$$\int_{\Omega} \mathcal{I}_h(f) \psi d\Omega = \int_{\Omega} \mathcal{I}_h(f\psi) d\Omega, \quad \forall \psi \in V_h^k.$$
 (21)

As a special case, we have

$$\int_{\Omega} \mathcal{I}_h(\phi \psi) d\Omega = \int_{\Omega} \phi \psi d\Omega, \quad \forall \psi, \phi \in V_h^k.$$
 (22)

Proof With similarity in technique, we will only show (21). It is sufficient to establish the results locally on each element. By the definition of \mathcal{I}_h^{ij} , and the key feature of the (k+1)-point Gaussian-Legendre quadrature rule that it is accurate for polynomials of degree up to 2k+1, we have $\forall \psi \in V_h^k$,

$$\begin{split} \int_{K_{ij}} \mathcal{I}_h^{ij}(f) \psi dx dy &= \frac{\Delta x_i}{2} \frac{\Delta y_j}{2} \sum_{m,n=0}^k \widehat{w}_m \widehat{w}_n \left(\mathcal{I}_h^{ij}(f) \psi \right) (x_{im}, y_{jn}) \\ &= \frac{\Delta x_i}{2} \frac{\Delta y_j}{2} \sum_{m,n=0}^k \widehat{w}_m \widehat{w}_n f(x_{im}, y_{jn}) \psi(x_{im}, y_{jn}) \\ &= \frac{\Delta x_i}{2} \frac{\Delta y_j}{2} \sum_{m,n=0}^k \widehat{w}_m \widehat{w}_n \mathcal{I}_h^{ij}(f \psi) (x_{im}, y_{jn}) = \int_{K_{ij}} \mathcal{I}_h^{ij}(f \psi) dx dy. \end{split}$$



Lemma 2 *Let* $f \in W_h(\Omega)$, then

$$\left| \int_{\Omega} \mathcal{I}_h(f) d\Omega \right| \le \int_{\Omega} \mathcal{I}_h(|f|) d\Omega. \tag{23}$$

If f is nonnegative, we also have

$$\int_{\Omega} \mathcal{I}_h(f) d\Omega \ge 0. \tag{24}$$

Proof The property can be showed by a direct calculation. For $f \in W_h(\Omega)$, we can see that

$$\pm \int_{\Omega} \mathcal{I}_{h}(f) d\Omega = \pm \sum_{i=1}^{N_{x}} \sum_{j=1}^{N_{y}} \frac{\Delta x_{i}}{2} \frac{\Delta y_{j}}{2} \sum_{m,n=0}^{k} \widehat{w}_{m} \widehat{w}_{n} (\mathcal{I}_{h}^{ij} f)(x_{im}, y_{jn})$$

$$= \pm \sum_{i=1}^{N_{x}} \sum_{j=1}^{N_{y}} \frac{\Delta x_{i}}{2} \frac{\Delta y_{j}}{2} \sum_{m,n=0}^{k} \widehat{w}_{m} \widehat{w}_{n} f(x_{im}, y_{jn})$$

$$\leq \sum_{i=1}^{N_{x}} \sum_{j=1}^{N_{y}} \frac{\Delta x_{i}}{2} \frac{\Delta y_{j}}{2} \sum_{m,n=0}^{k} \widehat{w}_{m} \widehat{w}_{n} |f|(x_{im}, y_{jn}) = \int_{\Omega} \mathcal{I}_{h}(|f|) d\Omega.$$

Here we have used the fact that the quadrature weights $\{\widehat{w}_m\}_{m=0}^k$ are positive. This implies (23). When f is nonnegative, (24) follows immediately from the above proof.

Semi-discrete in space methods. Now we are ready to present the semi-discrete in space schemes for the 2D model (17) based on nodal DG discretizations: find H_{zh} , E_h , D_h , J_h , P_h , σ_h and $Q_h \in V_h^k$, such that,

$$\mu_0(\partial_t H_{zh}, \phi) + \mathcal{B}_h^E(E_{xh}, E_{yh}, \phi) = 0, \quad \forall \phi \in V_h^k, \tag{25a}$$

$$(\partial_t D_{xh}, \phi) + \mathcal{B}_{xh}^H(H_{zh}, \phi) = 0, \quad \forall \phi \in V_h^k, \tag{25b}$$

$$(\partial_t D_{yh}, \phi) + \mathcal{B}_{vh}^H(H_{zh}, \phi) = 0, \quad \forall \phi \in V_h^k, \tag{25c}$$

$$\mathbf{D}_h = \epsilon_0 \Big(\epsilon_\infty \mathbf{E}_h + \mathbf{P}_h + a(1 - \theta) \mathcal{I}_h \Big(|\mathbf{E}_h|^2 \mathbf{E}_h \Big) + a\theta \mathcal{I}_h (Q_h \mathbf{E}_h) \Big), \tag{25d}$$

$$\partial_t \boldsymbol{P}_h = \boldsymbol{J}_h, \tag{25e}$$

$$\partial_t \mathbf{J}_h + \gamma \mathbf{J}_h + \omega_0^2 \mathbf{P}_h = \omega_p^2 \mathbf{E}_h, \tag{25f}$$

$$\partial_t Q_h = \sigma_h, \tag{25g}$$

$$\partial_t \sigma_h + \gamma_v \sigma_h + \omega_v^2 Q_h = \omega_v^2 \mathcal{I}_h(|E_h|^2). \tag{25h}$$

Here (\cdot, \cdot) is the standard L^2 inner product for $L^2(\Omega)$. The multilinear form $\mathcal{B}_h^E(\cdot, \cdot, \cdot)$ and bilinear forms $\mathcal{B}_{xh}^H(\cdot, \cdot)$ and $\mathcal{B}_{yh}^H(\cdot, \cdot)$ are

$$\mathcal{B}_{h}^{E}(E_{xh}, E_{yh}, \phi) = -\sum_{i=1}^{N_{x}} \int_{y_{a}}^{y_{b}} \widehat{E_{yh}}(x_{i+\frac{1}{2}}, y) [\phi]_{x_{i+\frac{1}{2}}} dy$$

$$+ \sum_{j=1}^{N_{y}} \int_{x_{a}}^{x_{b}} \widehat{\widehat{E_{xh}}}(x, y_{j+\frac{1}{2}}) [\phi]_{y_{j+\frac{1}{2}}} dx - (E_{yh}, \partial_{x}\phi) + (E_{xh}, \partial_{y}\phi),$$
(26a)



$$\mathcal{B}_{xh}^{H}(H_{zh},\phi) = \sum_{j=1}^{N_y} \int_{x_a}^{x_b} \widetilde{H_{zh}}(x,y_{j+\frac{1}{2}}) [\phi]_{y_{j+\frac{1}{2}}} dx + (H_{zh},\partial_y\phi), \tag{26b}$$

$$\mathcal{B}_{yh}^{H}(H_{zh},\phi) = -\sum_{i=1}^{N_x} \int_{y_a}^{y_b} \widetilde{H_{zh}}(x_{i+\frac{1}{2}},y)[\phi] x_{i+\frac{1}{2}} dy - (H_{zh},\partial_x\phi).$$
 (26c)

The numerical fluxes can be either central flux

(2021) 89:45

$$\widehat{E_{yh}}(x_{i+\frac{1}{2}}, y) = \{E_{yh}\}_{x_{i+\frac{1}{2}}}, \widehat{\widehat{E_{xh}}}(x, y_{j+\frac{1}{2}}) = \{E_{xh}\}_{y_{j+\frac{1}{2}}},$$
(27a)

$$\widetilde{H_{zh}}(x_{i+\frac{1}{2}}, y) = \{H_{zh}\}_{x_{i+\frac{1}{2}}}, \widetilde{\widetilde{H_{zh}}}(x, y_{j+\frac{1}{2}}) = \{H_{zh}\}_{y_{j+\frac{1}{2}}},$$
 (27b)

or alternating fluxes,

$$\widehat{E_{yh}}(x_{i+\frac{1}{2}}, y) = E_{yh}(x_{i+\frac{1}{2}}^{\dagger}, y), \ \widehat{\widehat{E_{xh}}}(x, y_{j+\frac{1}{2}}) = E_{xh}(x, y_{j+\frac{1}{2}}^{\sharp}),$$
(28a)

$$\widetilde{H_{zh}}(x_{i+\frac{1}{2}}, y) = H_{zh}(x_{i+\frac{1}{2}}^{\sharp}, y), \widetilde{\widetilde{H_{zh}}}(x, y_{j+\frac{1}{2}}) = H_{zh}(x, y_{j+\frac{1}{2}}^{\sharp}).$$
 (28b)

The following are required for the superscripts \dagger , \ddagger , \natural , \sharp in the alternating fluxes.

$$\dagger, \ddagger, \downarrow, \sharp \in \{+, -\}, \quad \dagger \text{ differs from } \sharp, \quad \natural \text{ differs from } \sharp.$$
 (29)

This in total will give us four possible choices of alternating fluxes. We particularly refer to the one with $\dagger = +, \ddagger = -, \ddagger = +, \ddagger = -$ as Alternating I, and the one with $\dagger = +, \ddagger =$ $-, \natural = -, \sharp = +$ as Alternating II.

The next lemma is a direct result of the choices of numerical fluxes, and it can be easily verified.

Lemma 3 With either central fluxes (27) or any set of alternating fluxes in (28)–(29), we have

$$\widehat{E_{yh}}[H_{zh}] + \widetilde{H_{zh}}[E_{yh}] = [E_{yh}H_{zh}] \text{ at } x = x_{i+\frac{1}{2}},$$

$$\widehat{\widehat{E_{xh}}}[H_{zh}] + \widetilde{H_{zh}}[E_{xh}] = [E_{xh}H_{zh}] \text{ at } y = y_{j+\frac{1}{2}}.$$

Moreover, under the assumption of periodic boundary conditions, we have

$$\mathcal{B}_{h}^{E}(\psi,\Phi,\phi) + \mathcal{B}_{xh}^{H}(\phi,\psi) + \mathcal{B}_{yh}^{H}(\phi,\Phi) = 0, \quad \forall \psi,\Phi,\phi \in V_{h}^{k}. \tag{30}$$

Energy stability and error estimates. For the semi-discrete in space methods in (25) with the numerical fluxes either in (27) or in (28)–(29), one can establish an energy relation similar as for the continuous model. Additionally, error estimates can be proved and they are optimal with respect to the approximation property of the discrete space V_h^k when the numerical fluxes are alternating.

Theorem 2 (Semi-discrete in space energy stability) Under the assumption of periodic boundary conditions, the semi-discrete in space methods (25), with either (27) or (28)–(29), satisfy

$$\frac{d\mathcal{E}_h(t)}{dt} = -\frac{\epsilon_0 \gamma}{\omega_p^2} \int_{\Omega} |\boldsymbol{J}_h|^2 d\Omega - \frac{\epsilon_0 a \theta \gamma_v}{2\omega_v^2} \int_{\Omega} \sigma_h^2 d\Omega \le 0, \tag{31}$$

with the discrete energy defined as

$$\mathcal{E}_{h} = \int_{\Omega} \left(\frac{\mu_{0}}{2} H_{zh}^{2} + \frac{\epsilon_{0} \epsilon_{\infty}}{2} |E_{h}|^{2} + \frac{\epsilon_{0}}{2\omega_{p}^{2}} |J_{h}|^{2} + \frac{\epsilon_{0} \omega_{0}^{2}}{2\omega_{p}^{2}} |P_{h}|^{2} + \frac{\epsilon_{0} a\theta}{4\omega_{v}^{2}} \sigma_{h}^{2} \right. \\
\left. + \frac{\epsilon_{0} a\theta}{2} \mathcal{I}_{h} \left(Q_{h} |E_{h}|^{2} \right) + \frac{3\epsilon_{0} a(1-\theta)}{4} \mathcal{I}_{h} \left(|E_{h}|^{4} \right) + \frac{\epsilon_{0} a\theta}{4} Q_{h}^{2} \right) d\Omega. \tag{32}$$

Moreover, when $\theta \in [0, \frac{3}{4}], \mathcal{E}_h \geq 0$.

Proof Take $\phi = H_{zh}$ in (25a), $\phi = E_{xh}$ in (25b) and $\phi = E_{yh}$ in (25c), using relation (30), we have

$$(\partial_t \mathbf{D}_h, \mathbf{E}_h) + \mu_0(\partial_t H_{zh}, H_{zh}) = 0. \tag{33}$$

Differentiate (25d) with respect to time t, one gets

$$(\partial_t \mathbf{D}_h, \mathbf{E}_h) = \epsilon_0 \epsilon_\infty (\partial_t \mathbf{E}_h, \mathbf{E}_h) + \epsilon_0 (\partial_t \mathbf{P}_h, \mathbf{E}_h) + \epsilon_0 a (1 - \theta) (\partial_t \mathcal{I}_h (|\mathbf{E}_h|^2 \mathbf{E}_h), \mathbf{E}_h) + \epsilon_0 a \theta (\partial_t \mathcal{I}_h (Q_h \mathbf{E}_h), \mathbf{E}_h).$$
(34)

Note that the operator ∂_t commutes with \mathcal{I}_h and with \int_{Ω} . With this and Lemma 1, the nonlinear Kerr term becomes

$$\left(\partial_{t} \mathcal{I}_{h}(|\boldsymbol{E}_{h}|^{2} \boldsymbol{E}_{h}), \boldsymbol{E}_{h}\right) = \int_{\Omega} \mathcal{I}_{h} \partial_{t}(|\boldsymbol{E}_{h}|^{2} \boldsymbol{E}_{h}) \cdot \boldsymbol{E}_{h} d\Omega$$

$$= \int_{\Omega} \mathcal{I}_{h} \left(\partial_{t}(|\boldsymbol{E}_{h}|^{2} \boldsymbol{E}_{h}) \cdot \boldsymbol{E}_{h}\right) d\Omega = \frac{3}{4} \frac{d}{dt} \int_{\Omega} \mathcal{I}_{h}(|\boldsymbol{E}_{h}|^{4}) d\Omega. \quad (35)$$

Similarly, for the nonlinear Raman term, one has

$$\begin{aligned}
\left(\partial_{t} \mathcal{I}_{h}(Q_{h} \boldsymbol{E}_{h}), \boldsymbol{E}_{h}\right) &= \int_{\Omega} \mathcal{I}_{h} \left(\partial_{t}(Q_{h} \boldsymbol{E}_{h}) \cdot \boldsymbol{E}_{h}\right) d\Omega \\
&= \frac{1}{2} \int_{\Omega} \mathcal{I}_{h} \left(\partial_{t}(Q_{h} |\boldsymbol{E}_{h}|^{2}) + \partial_{t} Q_{h} |\boldsymbol{E}_{h}|^{2}\right) d\Omega \\
&= \frac{1}{2} \frac{d}{dt} \int_{\Omega} \mathcal{I}_{h}(Q_{h} |\boldsymbol{E}_{h}|^{2}) d\Omega + \frac{1}{2} \int_{\Omega} \partial_{t} Q_{h} |\boldsymbol{I}_{h}(|\boldsymbol{E}_{h}|^{2}) d\Omega.
\end{aligned} \tag{36}$$

The second term in (36) can be reformulated by further using (25g)–(25h),

$$\int_{\Omega} \partial_t Q_h \mathcal{I}_h \left(|\boldsymbol{E}_h|^2 \right) d\Omega = \frac{1}{\omega_v^2} \int_{\Omega} \partial_t Q_h \left(\partial_t \sigma_h + \gamma_v \sigma_h + \omega_v^2 Q_h \right) d\Omega
= \frac{1}{2\omega_v^2} \frac{d}{dt} \int_{\Omega} \sigma_h^2 d\Omega + \frac{\gamma_v}{\omega_v^2} \int_{\Omega} \sigma_h^2 d\Omega + \frac{1}{2} \frac{d}{dt} \int_{\Omega} Q_h^2 d\Omega.$$
(37)

For the Lorentz term, using (25e)–(25f), we reach

$$(\partial_t \boldsymbol{P}_h, \boldsymbol{E}_h) = \frac{1}{\omega_p^2} \int_{\Omega} \partial_t \boldsymbol{P}_h \cdot \left(\partial_t \boldsymbol{J}_h + \gamma \boldsymbol{J}_h + \omega_0^2 \boldsymbol{P}_h \right) d\Omega$$

$$= \frac{1}{2\omega_p^2} \frac{d}{dt} \int_{\Omega} |\boldsymbol{J}_h|^2 d\Omega + \frac{\gamma}{\omega_p^2} \int_{\Omega} |\boldsymbol{J}_h|^2 d\Omega + \frac{\omega_0^2}{2\omega_p^2} \frac{d}{dt} \int_{\Omega} |\boldsymbol{P}_h|^2 d\Omega. \tag{38}$$

We now can combine (33)–(38) and conclude the energy relation (31) with \mathcal{E}_h defined in (32).



Finally, using (22) from Lemma 1 and (24) from Lemma 2, we can see that, under the condition $\theta \in [0, \frac{3}{d}]$, the discrete energy (32) is non-negative, i.e.,

$$\begin{split} \mathcal{E}_h &= \int_{\Omega} \left(\frac{\mu_0}{2} H_{zh}^2 + \frac{\epsilon_0 \epsilon_{\infty}}{2} |\boldsymbol{E}_h|^2 + \frac{\epsilon_0}{2\omega_p^2} |\boldsymbol{J}_h|^2 + \frac{\epsilon_0 \omega_0^2}{2\omega_p^2} |\boldsymbol{P}_h|^2 + \frac{\epsilon_0 a\theta}{4\omega_v^2} \sigma_h^2 \right. \\ &\quad + \frac{\epsilon_0 a\theta}{4} \mathcal{I}_h \left((|\boldsymbol{E}_h|^2 + Q_h)^2 \right) + \frac{\epsilon_0 a(3 - 4\theta)}{4} \mathcal{I}_h \left(|\boldsymbol{E}_h|^4 \right) \right) \! d\Omega \geq 0. \end{split}$$

Based on the energy stability in Theorem 2 and the approximation property of V_h^k (see "Appendix A"), we can further establish error estimates for the semi-discrete in space DG methods. The proof will be given in "Appendix A", and it follows similar steps as that in [3] for the 1D version of the models considered here, with special attention paid to the nodal form of DG spatial discretizations dealing with nonlinearity and to the use of interpolation operators.

Theorem 3 (Semi-discrete in space error estimates) Let T > 0 be given. Let $\kappa_{err} \in (0, 1)$, $\rho_{err} \in (0, 1)$ be arbitrary constants, then under periodic boundary conditions and

• Condition 1:

$$\theta \in \left[0, \frac{1}{1 + 3(1 - \rho_{err})^{-2}}\right],$$
(39)

• Condition 2:

$$a\theta C_k \|Q\|_{\infty} \le \epsilon_{\infty} (1 - \kappa_{err}),\tag{40}$$

• Condition 3:

$$a\left(12(1-\theta)C_k^2 \|\boldsymbol{E}\|_{\infty} \|\partial_t \boldsymbol{E}\|_{\infty} + (12-11\theta)\frac{C_k^2}{\rho_{err}} \|\partial_t \boldsymbol{E}\|_{\infty}^2 + 2\theta C_k \|\partial_t Q\|_{\infty}\right) \leq \epsilon_{\infty} \kappa_{err},$$
(41)

as well as the exact solution being sufficiently smooth, the numerical solution u_h given by (25) with suitable initialization (i.e. specified in the proof) admits the following error estimate,

$$||u - u_h||(T) \le CC(\kappa_{err}, \rho_{err})h^r, u = H_z, \boldsymbol{E}, \boldsymbol{P}, \boldsymbol{J}, \sigma, Q,$$

with

$$r = \begin{cases} k, & \textit{for central numerical fluxes,} \\ k+1, \textit{for alternating numerical fluxes.} \end{cases}$$

Throughout this paper, $\|\cdot\|$ and $\|\cdot\|_{\infty}$ will be used to denote the standard L^2 norm and L^{∞} norm. C is a generic constant independent of h, but may depend on k, the mesh parameter δ , the model parameters, and some Sobolev norm of the exact solutions up to time T. We also denote by C_{\star} a generic constant which may depend on k and the mesh parameter δ and by C_k a usually computable constant depending only on k. These constants may take different values at their different appearances.

Remark 1 For the semi-discrete in space DG methods on Cartesian meshes with any alternating fluxes, it is necessary to use Q^k -type elements to obtain optimal error estimates, as previously analyzed in [20]. The proof of our optimality relies on a super-convergence result



from [20]. If the P^k -type discrete space is employed (that is, the space with approximating functions being polynomials of total degree up to k on each element), only sub-optimal error estimates can be obtained. Indeed, even for the 2D TE model of the Maxwell's equations in the simple linear media with (17d) replaced by $D = \epsilon_0 \epsilon_\infty E$, both E_x and E_y are numerically observed to be k-th order accurate when DG methods are used with the P^k -type discrete space and alternating numerical fluxes.

Remark 2 There are three conditions in Theorem 3. Condition 1 essentially requires $\theta \in [0, \frac{1}{4}]$, and this is more stringent than the required range, $\theta \in [0, \frac{3}{4}]$, in Theorem 2 for energy stability. Conditions 2-3 require the smallness of the strength of the nonlinearity, and depend on some constant C_k . These sufficient conditions may not be necessary for the error estimates to hold.

2.3 Fully-Discrete Methods

Combining the strategies of temporal and spatial discretizations as well as the nonlinear treatments in Sects. 2.1–2.2, we arrive at the fully-discrete leap-frog nodal DG schemes: given H^n_{zh} , E^n_h , D^n_h , J^n_h , P^n_h , σ^n_h and $Q^n_h \in V^k_h$ at time $t = t^n$, we find H^{n+1}_{zh} , E^{n+1}_h , D^{n+1}_h , J^{n+1}_h , D^{n+1}_h , σ^{n+1}_h and $Q^{n+1}_h \in V^k_h$ at time $t^{n+1} = t^n + \Delta t$, satisfying

$$\mu_0\left(\frac{H_{zh}^{n+1/2} - H_{zh}^n}{\Delta t/2}, \phi\right) + \mathcal{B}_h^E(E_{xh}^n, E_{yh}^n, \phi) = 0, \quad \forall \phi \in V_h^k, \tag{42a}$$

$$\left(\frac{D_{xh}^{n+1} - D_{xh}^{n}}{\Delta t}, \phi\right) + \mathcal{B}_{xh}^{H}(H_{zh}^{n+1/2}, \phi) = 0, \quad \forall \phi \in V_h^k, \tag{42b}$$

$$\left(\frac{D_{yh}^{n+1} - D_{yh}^{n}}{\Delta t}, \phi\right) + \mathcal{B}_{yh}^{H}(H_{zh}^{n+1/2}, \phi) = 0, \quad \forall \phi \in V_{h}^{k}, \tag{42c}$$

$$\boldsymbol{D}_h^{n+1} = \epsilon_0 \left(\epsilon_\infty \boldsymbol{E}_h^{n+1} + \boldsymbol{P}_h^{n+1} + a(1-\theta)\boldsymbol{Y}_h^{n+1} + a\theta \mathcal{I}_h \left(\boldsymbol{Q}_h^{n+1} \boldsymbol{E}_h^{n+1} \right) \right),$$

$$\boldsymbol{Y}_{h}^{n+1} = \boldsymbol{Y}_{h}^{n} + \mathcal{I}_{h} \left(\left(|\boldsymbol{E}_{h}^{n+1}|^{2} + |\boldsymbol{E}_{h}^{n}|^{2} - \boldsymbol{E}_{h}^{n+1} \cdot \boldsymbol{E}_{h}^{n} \right) \left(\boldsymbol{E}_{h}^{n+1} - \boldsymbol{E}_{h}^{n} \right) \right)$$
(42d)

$$+\frac{1}{2}\mathcal{I}_{h}\left((\boldsymbol{E}_{h}^{n+1}+\boldsymbol{E}_{h}^{n})\cdot(\boldsymbol{E}_{h}^{n+1}-\boldsymbol{E}_{h}^{n})(\boldsymbol{E}_{h}^{n+1}+\boldsymbol{E}_{h}^{n})\right),\tag{42e}$$

$$\frac{P_h^{n+1} - P_h^n}{\Delta t} = \frac{J_h^{n+1} + J_h^n}{2},\tag{42f}$$

$$\frac{\boldsymbol{J}_{h}^{n+1} - \boldsymbol{J}_{h}^{n}}{\Delta t} + \gamma \frac{\boldsymbol{J}_{h}^{n+1} + \boldsymbol{J}_{h}^{n}}{2} + \omega_{0}^{2} \frac{\boldsymbol{P}_{h}^{n+1} + \boldsymbol{P}_{h}^{n}}{2} = \omega_{p}^{2} \frac{\boldsymbol{E}_{h}^{n+1} + \boldsymbol{E}_{h}^{n}}{2}, \tag{42g}$$

$$\frac{Q_h^{n+1} - Q_h^n}{\Delta t} = \frac{\sigma_h^{n+1} + \sigma_h^n}{2},\tag{42h}$$

$$\frac{\sigma_h^{n+1} - \sigma_h^n}{\Delta t} + \gamma_v \frac{\sigma_h^{n+1} + \sigma_h^n}{2} + \omega_v^2 \frac{Q_h^{n+1} + Q_h^n}{2} = \omega_v^2 \mathcal{I}_h(E_h^{n+1} \cdot E_h^n), \tag{42i}$$

$$\mu_0\left(\frac{H_{zh}^{n+1}-H_{zh}^{n+1/2}}{\Delta t/2},\phi\right)+\mathcal{B}_h^E(E_{xh}^{n+1},E_{yh}^{n+1},\phi)=0,\quad\forall\phi\in V_h^k. \tag{42j}$$

The terms of \mathcal{B}_h^E , \mathcal{B}_{xh}^H , and \mathcal{B}_{yh}^H are defined in (26), with either the central fluxes (27) or alternating fluxes in (28)–(29).



Just as for the semi-discrete methods in Sects. 2.1–2.2, we will see next in Theorem 4 that the fully-discrete methods satisfy a provable energy relation. By further requiring the discrete energy to be non-negative, the CFL condition on the allowable time step size is identified for energy stability. The condition turns out to be the same when the proposed methods are adapted to the linear Maxwell's equations with the constitutive law $D = \epsilon_0 \epsilon_\infty E$. The main factors that contribute to the energy relation in Theorem 4 are outlined in the proofs of energy results for semi-discrete methods, and the new aspect is to obtain the time step condition.

Theorem 4 (Fully-discrete energy stability) *Under the assumption of periodic boundary conditions, the fully-discrete leap-frog nodal DG schemes* (42) *satisfy*

$$\mathcal{E}_{h}^{n+1} - \mathcal{E}_{h}^{n} = -\frac{\epsilon_{0}\gamma \Delta t}{4\omega_{p}^{2}} \int_{\Omega} |\boldsymbol{J}_{h}^{n+1} + \boldsymbol{J}_{h}^{n}|^{2} d\Omega - \frac{\epsilon_{0}a\theta\gamma_{v}\Delta t}{8\omega_{v}^{2}} \int_{\Omega} (\sigma_{h}^{n+1} + \sigma_{h}^{n})^{2} d\Omega \leq 0,$$

$$\tag{43}$$

with the discrete energy \mathcal{E}_h^n defined as

$$\mathcal{E}_{h}^{n} = \int_{\Omega} \left(\frac{\mu_{0}}{2} H_{zh}^{n+1/2} H_{zh}^{n-1/2} + \frac{\epsilon_{0} \epsilon_{\infty}}{2} \left| \boldsymbol{E}_{h}^{n} \right|^{2} + \frac{\epsilon_{0}}{2\omega_{p}^{2}} \left| \boldsymbol{J}_{h}^{n} \right|^{2} + \frac{\epsilon_{0} \omega_{0}^{2}}{2\omega_{p}^{2}} \left| \boldsymbol{P}_{h}^{n} \right|^{2} + \frac{\epsilon_{0} a \theta}{4\omega_{v}^{2}} \left(\sigma_{h}^{n} \right)^{2} + \frac{\epsilon_{0} a \theta}{4} \mathcal{I}_{h} \left(\left| \boldsymbol{E}_{h}^{n} \right|^{4} \right) + \frac{\epsilon_{0} a \theta}{4} \left(\left| \boldsymbol{Q}_{h}^{n} \right|^{2} \right) d\Omega. \tag{44}$$

Moreover, $\mathcal{E}_h^n \geq 0$ if $\theta \in [0, \frac{3}{4}]$ and under the following time step condition

$$\frac{\Delta t}{h} \le \min\left(\frac{\mu_0}{C_{\star}}, \frac{\epsilon_0 \epsilon_{\infty}}{C_{\star}}\right).$$

Proof See "Appendix B".

Remark 3 Thanks to the explicit treatment of the PDE part in our schemes, at each time step, one can solve the nonlinear ODEs for E^{n+1} , P^{n+1} , J^{n+1} , Q^{n+1} and σ^{n+1} locally in each element. If DG spatial discretizations are in modal form, this will result in a nonlinear algebraic system of $(3d+2) \times (k+1)^2$ equations and unknowns for each element K_{ij} . Here again d is the spatial dimension. The nodal form adopted in this work however will decouple this large system into $(k+1)^2$ smaller nonlinear algebraic systems, with each involving (3d+2) equations and unknowns related to each interpolation point (x_{im}, y_{jn}) in K_{ij} . This will be computationally much more efficient. For each of such nonlinear systems, one can further eliminate P^{n+1} , P^{n+1} , P^{n+1} and P^{n+1} analytically, and this will lead to an even smaller cubic nonlinear system that only involves the P^{n+1} unknown components of P^{n+1} . One can refer to Sect. 3.1 for numerical illustration and comparison.

3 Numerical Examples

In this section, we carry out a set of numerical experiments to validate the performance of our proposed schemes. These tests are performed on the model (1) in its nondimensionlized form,

$$\partial_t \mathbf{H} + \nabla \times \mathbf{E} = \mathbf{0},\tag{45a}$$

$$\partial_t \mathbf{D} - \nabla \times \mathbf{H} = \mathbf{0},\tag{45b}$$

$$\mathbf{D} = \epsilon_{\infty} \mathbf{E} + \mathbf{P} + a(1 - \theta)|\mathbf{E}|^2 \mathbf{E} + a\theta Q \mathbf{E}, \tag{45c}$$



$$\partial_t \mathbf{P} = \mathbf{J},\tag{45d}$$

$$\partial_t \mathbf{J} + \gamma \mathbf{J} + \omega_0^2 \mathbf{P} = \omega_n^2 \mathbf{E},\tag{45e}$$

$$\partial_t Q = \sigma,$$
 (45f)

$$\partial_t \sigma + \gamma_v \sigma + \omega_v^2 Q = \omega_v^2 |E|^2. \tag{45g}$$

The initialization at t=0 is via the interpolation, namely, $u_h(\cdot, \cdot, 0) = \mathcal{I}_h u(\cdot, \cdot, 0)$, with u being any of the unknown quantity. A nonlinear algebraic system $F(u^s) = \mathbf{0}$ needs to be solved at each interpolation point, see Remark 3. For each of them, we use Newton's iteration method, with the stopping criterion $||F(u^s)||_{\infty} < Err_{tol}$, where Err_{tol} is a chosen error tolerance. Due to the small size of each nonlinear system, in our simulations the Gaussian elimination method is applied to solve the linearized system during each Newton's iteration.

3.1 Accuracy, Computational Efficiency, Energy Stability

In this subsection, we present an example with manufactured solutions to demonstrate the accuracy and computational efficiency of the proposed schemes. We also numerically examine the energy stability (more accurately, the energy conservation in a conservative medium). Let $\Omega = [0, \frac{2\pi}{\alpha w}] \times [0, \frac{2\pi}{\beta w}]$, where $\alpha = \cos(0.3\pi)$, $\beta = \sin(0.3\pi)$, w = 1.0. The model parameters are set as: $\epsilon_{\infty} = 1.0$, $\omega_0 = \omega_p = 1.0$, $\gamma = 0.05$, $\alpha = 1/3$, $\theta = 0.5$, $\omega_v = 1.0$, $\gamma = 0.05$. We use the following functions as the manufactured solutions:

$$\begin{cases}
H_z = e^{\cos(w(t+\alpha x+\beta y))}, \\
E_x = \beta e^{\cos(w(t+\alpha x+\beta y))}, \\
E_y = -\alpha e^{\cos(w(t+\alpha x+\beta y))}, \\
P_x = E_x, J_x = \partial_t P_x, \\
P_y = E_y, J_y = \partial_t P_y, \\
D_x = E_x, \\
D_y = E_y, \\
Q = H_z, \sigma = \partial_t Q,
\end{cases}$$
(46)

which satisfy the PDE part of the system (45) exactly. For equation balance, suitable source functions are added to the rest of the system (i.e. the constitutive law, the ODE part), and they are evaluated at $(t^n + t^{n+1})/2$ when the solutions are numerically updated from t^n to t^{n+1} . Periodic boundary conditions are applied in space, and the final time is T = 1. The nonlinear stopping criteria in Newton's iterations is $Err_{tol} = 10^{-12}$. To match the high order accuracy in space and avoid the influence on the accuracy caused by time step changes, we first set

$$dt = \Theta h^{\frac{k+1}{2}}, \ h = \frac{1}{2\left(\frac{1}{\Delta x} + \frac{1}{\Delta y}\right)},$$

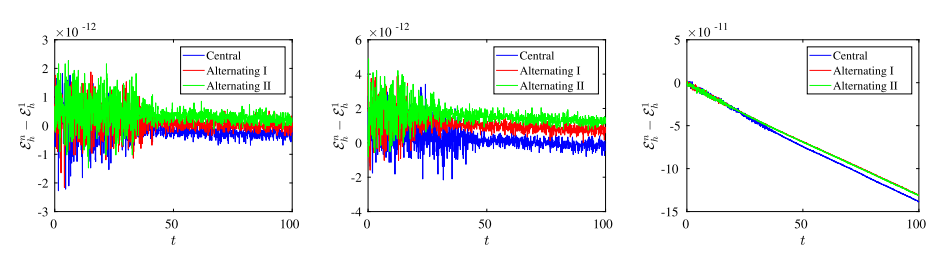
with constant Θ chosen as

$$\Theta = \begin{cases} 0.3, & k = 1, \\ 1.0, & k = 2, \\ 2.0, & k = 3, \end{cases}$$

and then adjust the time step as $\Delta t = \frac{T}{\lceil T/dt \rceil + 1}$ to ensure uniform time stepping.

In Tables 1-3, we report the L^2 and L^{∞} errors and order of convergence rates for our schemes when Q^k elements are used, k = 1, 2, 3. Since the results are similar with all four alternating numerical fluxes, we only include the results for the Alternating I & II numerical





(2021) 89:45

Fig. 1 The time history of energy deviation $\mathcal{E}_h^n - \mathcal{E}_h^1$. Left: k = 1, Middle: k = 2, Right: k = 3. Mesh: 80×80 .

fluxes. From Tables 1-2, one can observe the optimal accuracy of the schemes with both alternating numerical fluxes and Q^k elements. Results in Table 3 are for central flux, and one can observe the optimal accuracy for k = 2 and sub-optimal accuracy for k = 1, 3. All these results confirm or complement our theoretical error analysis.

We next want to demonstrate the computational efficiency of the nodal form of DG schemes by comparing them with the modal form of the DG schemes. As commented in Remark 3, with the modal form of the DG schemes, one needs to solve one nonlinear algebraic system of $(3d+2) \times (k+1)^2$ equations and unknowns per mesh element, while the nodal form of the DG methods decouples the system into $(k+1)^{2}$ smaller individual nonlinear equations, with each of size (3d + 2). The computational times of the corresponding algorithms in 2D with d=2 are reported in Table 4, under the column "time (s)", together with the L^2 errors of H_{τ} . One can see that the nodal and modal DG schemes give almost identical numerical errors, with the former nearly 15 times, 80 times, 500 times faster for k = 1, 2, 3, respectively. Recall that during one Newton's iteration, with Gaussian elimination as the linear solver, the computational complexity for the modal DG method is about $(k+1)^4$ (i.e. 16, 81, 256 for k = 1, 2, 3, respectively) times of that for the nodal DG method. As suggested in Remark 3, within the nodal framework, one can further eliminate all other unknowns and solve a nonlinear system only for the d unknown components of E. This will lead to additional 2-3 times of reduction in the computational cost, which is reported under the column "time* (s)" in Table 4.

At last, we will examine the energy stable property of the schemes. To this end, we set $\gamma = \gamma_v = 0$, so the model is indeed energy conserving as in (3). The initial conditions are taken to be the same as those used in the accuracy test, yet the external source terms are switched off in the simulation for energy conservation. Again boundary conditions are periodic in space. We run the simulations up to the final time T = 100 on a 80×80 mesh.

By Theorem 4, the fully-discrete schemes will be energy conserving, namely, $\mathcal{E}_h^{n+1} - \mathcal{E}_h^n =$ 0, with

$$\begin{split} \mathcal{E}_{h}^{n} &= \int_{\Omega} \left(\frac{1}{2} H_{zh}^{n+1/2} H_{zh}^{n-1/2} + \frac{\epsilon_{\infty}}{2} \left| \boldsymbol{E}_{h}^{n} \right|^{2} + \frac{1}{2\omega_{p}^{2}} \left| \boldsymbol{J}_{h}^{n} \right|^{2} + \frac{\omega_{0}^{2}}{2\omega_{p}^{2}} \left| \boldsymbol{P}_{h}^{n} \right|^{2} + \frac{a\theta}{4\omega_{v}^{2}} \left(\sigma_{h}^{n} \right)^{2} \right. \\ &+ \left. \frac{a\theta}{2} \mathcal{I}_{h} \left(Q_{h}^{n} | \boldsymbol{E}_{h}^{n} |^{2} \right) + \frac{3a(1-\theta)}{4} \mathcal{I}_{h} \left(\left| \boldsymbol{E}_{h}^{n} \right|^{4} \right) + \frac{a\theta}{4} \left(Q_{h}^{n} \right)^{2} \right) d\Omega. \end{split}$$

This property is validated by the time evolution history of $\mathcal{E}_h^n - \mathcal{E}_h^1$ in Fig. 1 for both alternating and central fluxes and with Q^k elements, k = 1, 2, 3. Recall that the error tolerance in Newton's iterations is 10^{-12} in this experiment, while the simulation is carried out in double precision.



Table 1 Numerical errors and convergence rates: Alternating I flux

Mesh	E_x				E_y				H_{z}			
	L^2		T_{∞}		L^2		T_{∞}		L^2		T_{∞}	
Q^1												
20×20	8.79E-03	ı	5.59E-02	ı	6.02E-03	ı	4.63E-02	ı	1.32E-02	ı	9.08E-02	ı
40×40	2.18E-03	2.01	1.40E-02	2.00	1.68E-03	1.84	1.14E-02	2.02	3.61E-03	1.87	2.30E-02	1.98
80×80	5.30E-04	2.04	3.42E-03	2.04	4.17E-04	2.01	2.72E-03	2.07	7.86E-04	2.20	5.56E-03	2.05
160×160	1.37E-04	1.96	8.84E-04	1.95	1.10E-04	1.92	7.32E-04	1.89	2.08E-04	1.92	1.45E-03	1.94
320×320	3.38E-05	2.02	2.23E-04	1.99	2.77E-05	1.99	1.86E-04	1.98	5.54E-05	1.91	3.77E-04	1.94
Q^2												
20×20	3.91E-04	1	2.35E-03	ı	3.30E-04	1	2.08E-03	ı	7.06E-04	ı	6.12E-03	1
40×40	4.62E-05	3.08	2.62E-04	3.16	3.94E-05	3.06	2.53E-04	3.04	8.51E-05	3.05	5.46E-04	3.49
80×80	5.65E-06	3.03	3.51E-05	2.90	4.56E-06	3.11	2.60E-05	3.28	9.25E-06	3.20	6.52E-05	3.07
160×160	7.13E-07	2.99	4.26E-06	3.04	5.61E-07	3.02	3.83E-06	2.76	1.32E-06	2.81	1.27E-05	2.36
320×320	8.98E-08	2.99	6.04E-07	2.82	7.22E-08	2.96	4.64E-07	3.05	1.60E-07	3.05	1.16E-06	3.46
Q^3												
20×20	2.39E-05	1	1.33E-04	ı	1.86E-05	1	9.42E-05	ı	8.24E-05	ı	3.58E-04	1
40×40	1.51E-06	3.98	7.47E-06	4.16	1.14E-06	4.03	6.25E-06	3.91	5.15E-06	4.00	2.42E-05	3.89
80×80	9.52E-08	3.99	4.80E-07	3.96	7.25E-08	3.97	4.17E-07	3.91	3.26E-07	3.98	1.60E-06	3.92
160×160	5.97E-09	4.00	3.57E-08	3.75	4.53E-09	4.00	3.33E-08	3.65	2.04E-08	3.99	9.56E-08	4.06
320×320	3.75E-10	3.99	2.63E-09	3.76	2.84E-10	4.00	2.00E-09	4.06	1.27E-09	4.00	6.20E-09	3.95



 $\textbf{Table 2}~\mbox{Numerical errors}$ and convergence rates: Alternating II flux

Mesh	E_x				$E_{\rm y}$				$H_{\tilde{z}}$			
	L^2		Γ_{∞}		L^2		T_{∞}		L^2		Γ_{∞}	
Q^1												
20×20	7.68E-03	I	6.12E-02	I	5.77E-03	I	4.28E-02	I	1.54E-02	I	9.65E-02	I
40×40	2.62E-03	1.55	1.57E-02	1.96	1.60E-03	1.85	1.02E-02	2.07	3.30E-03	2.22	2.26E-02	2.10
80×80	5.57E-04	2.23	4.05E-03	1.96	3.99E-04	2.01	2.66E-03	1.93	8.32E-04	1.99	5.14E-03	2.13
160×160	1.49E-04	1.90	1.01E-03	2.00	1.05E-04	1.93	6.66E-04	2.00	2.18E-04	1.93	1.47E-03	1.81
320×320	3.86E-05	1.95	2.64E-04	1.94	2.67E-05	1.98	1.83E-04	1.87	5.35E-05	2.02	3.58E-04	2.04
Q^2												
20×20	4.61E-04	,	4.34E-03	ı	3.18E-04	ı	2.02E-03	ı	6.17E-04	ı	3.42E-03	ı
40×40	5.71E-05	3.02	4.57E-04	3.24	3.78E-05	3.07	2.76E-04	2.87	6.87E-05	3.17	3.72E-04	3.20
80×80	6.27E-06	3.19	4.61E-05	3.31	4.19E-06	3.17	2.96E-05	3.22	8.49E-06	3.02	5.65E-05	2.72
160×160	8.69E-07	2.85	7.88E-06	2.55	5.20E-07	3.01	3.70E-06	3.00	1.13E-06	2.91	7.94E-06	2.83
320×320	1.08E-07	3.01	9.99E-07	2.98	6.75E-08	2.95	4.54E-07	3.03	1.35E-07	3.06	9.05E-07	3.13
Q^3												
20×20	2.52E-05	ı	1.30E-04	ı	1.84E-05	ı	9.93E-05	ı	8.13E-05	ı	3.17E-04	ı
40×40	1.55E-06	4.02	8.87E-06	3.88	1.11E-06	4.05	5.92E-06	4.07	5.10E-06	4.00	1.88E-05	4.08
80×80	9.76E-08	3.99	6.27E-07	3.82	7.13E-08	3.96	4.11E-07	3.85	3.21E-07	3.99	1.30E-06	3.85
160×160	6.09E-09	4.00	4.00E-08	3.97	4.46E-09	4.00	2.43E-08	4.08	2.01E-08	4.00	7.64E-08	4.09
320×320	3.81E-10	4.00	2.42E-09	4.04	2.79E-10	4.00	1.62E-09	3.90	1.25E-09	4.00	4.84E-09	3.98



Table 3 Numerical errors and convergence rates: Central flux

Mesh	E_x				E_{y}				H_z			
	L^2		Γ_{∞}		L^2		Γ_{∞}		L^2		Γ_{∞}	
Q^1												
20×20	2.45E-02	ı	8.30E-02	ı	1.96E-02	ı	6.74E-02	ı	3.96E-02	ı	1.66E-01	ı
40×40	1.22E-02	1.00	4.07E-02	1.03	9.84E-03	0.99	3.13E-02	1.11	1.98E-02	1.00	7.65E-02	1.11
80×80	6.13E-03	1.00	2.00E-02	1.02	4.93E-03	1.00	1.54E-02	1.03	9.91E-03	1.00	3.68E-02	1.06
160×160	3.06E-03	1.00	9.90E-03	1.01	2.47E-03	1.00	7.64E-03	1.01	4.96E-03	1.00	1.81E-02	1.03
320×320	1.53E-03	1.00	4.93E-03	1.01	1.24E-03	1.00	3.81E-03	1.00	2.48E-03	1.00	8.95E-03	1.01
Q^2												
20×20	2.56E-04	,	1.82E-03	,	1.86E-04	1	1.33E-03	1	3.56E-04	ı	2.36E-03	ı
40×40	2.90E-05	3.14	2.13E-04	3.09	2.14E-05	3.12	1.59E-04	3.06	3.99E-05	3.16	2.80E-04	3.07
80×80	3.59E-06	3.01	2.71E-05	2.97	2.61E-06	3.03	1.94E-05	3.04	4.91E-06	3.02	3.30E-05	3.09
160×160	4.47E-07	3.01	3.35E-06	3.02	3.25E-07	3.01	2.44E-06	2.99	6.13E-07	3.00	4.10E-06	3.01
320×320	5.58E-08	3.00	4.19E-07	3.00	4.06E-08	3.00	3.07E-07	2.99	7.66E-08	3.00	5.15E-07	2.99
Q^3												
20×20	3.94E-05	ı	1.56E-04	ı	2.56E-05	ı	1.05E-04	ı	8.84E-05	ı	2.82E-04	1
40×40	3.70E-06	3.41	2.02E-05	2.95	3.29E-06	2.96	1.30E-05	3.02	7.84E-06	3.50	4.08E-05	2.79
80×80	4.29E-07	3.11	2.20E-06	3.19	4.09E-07	3.01	1.84E-06	2.82	8.27E-07	3.25	5.17E-06	2.98
160×160	5.30E-08	3.02	2.96E-07	2.90	5.11E-08	3.00	2.40E-07	2.94	9.81E-08	3.08	6.44E-07	3.00
320×320	6.62E-09	3.00	3.61E-08	3.03	6.39E-09	3.00	3.04E-08	2.98	1.21E-08	3.02	8.04E-08	3.00



Mesh	Modal DG		Nodal DG		
	L^2	Time (s)	L^2	Time (s)	Time* (s)
Q^1					
20×20	1.32E-02	0.33	1.32E-02	0.02	0.01
40×40	3.61E-03	2.45	3.61E-03	0.16	0.05
80×80	7.86E-04	17.19	7.86E-04	1.23	0.43
Q^2					
20×20	7.01E-04	5.00	7.06E-04	0.04	0.02
40×40	8.51E-05	48.29	8.51E-05	0.44	0.17
80×80	9.26E-06	449.94	9.25E-06	5.10	1.98
Q^3					
20×20	8.24E-05	65.63	8.24E-05	0.10	0.04
40×40	5.15E-06	872.03	5.15E-06	1.74	0.67

 Table 4 Errors of H_Z and the elapsed CPU time for simulation: Alternating I flux

3.2 Physically Relevant Simulations

In this subsection, we apply the proposed schemes to simulate physically relevant problems. For the ease of illustration, the setup of the example and numerical results are presented in the dimensional form, though the actual simulation is conducted based on the nondimensionalized form. The results reported here are obtained by Q^2 approximations on a uniform mesh with $h=\Delta x=\Delta y=20$ nm and the time stepsize $\Delta t=0.05\sqrt{\epsilon_0\epsilon_\infty\mu_0}h$. The stopping criteria in the Newton's iteration is set as $Err_{tol}=10^{-8}$.

3.2.1 Spatial Optical Soliton Propagation

We first consider the spatial optical soliton propagation in realistic glasses. These glasses are characterized by a three-pole Sellmeier linear dispersion, an instantaneous Kerr nonlinearity and a dispersive Raman nonlinearity [15], modeled by

$$\mu_0 \partial_t H_z + \partial_x E_y - \partial_y E_x = 0, \tag{47a}$$

$$\partial_t D_x - \partial_y H_z = 0, (47b)$$

$$\partial_t D_v + \partial_x H_z = 0, (47c)$$

$$\mathbf{D} = \epsilon_0 \left(\epsilon_\infty \mathbf{E} + b \sum_{s=1}^3 \mathbf{P}_s + a(1-\theta) |\mathbf{E}|^2 \mathbf{E} + a\theta Q \mathbf{E} \right), \tag{47d}$$

$$\partial_{tt} \mathbf{P}_s + \gamma_s \partial_t \mathbf{P}_s + \omega_{0s}^2 \mathbf{P}_s = \omega_{ps}^2 \mathbf{E}, \quad s = 1, 2, 3, \tag{47e}$$

$$\partial_{tt} Q + \gamma_v \partial_t Q + \omega_v^2 Q = \omega_v^2 |E|^2. \tag{47f}$$

where

$$\omega_{01} = 2.7537 \times 10^{16} \text{ rad/s}, \ \omega_{02} = 1.6205 \times 10^{16} \text{ rad/s}, \ \omega_{03} = 1.9034 \times 10^{14} \text{ rad/s},$$

 $\beta_1 = 0.69617, \ \beta_2 = 0.40794, \ \beta_3 = 0.89748, \ \omega_{ps} = \sqrt{\beta_s}\omega_{0s}, \ \gamma_s = 0, s = 1, 2, 3,$
 $\epsilon_{\infty} = 1.0, \ b = 1.0, \ a = 1.89 \times 10^{-22} m^2 / V^2, \ \theta = 0.3,$



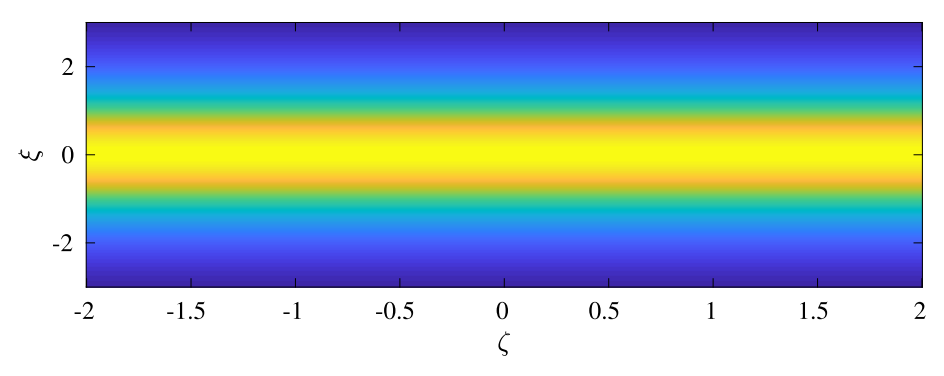


Fig. 2 Fundamental soliton $|u_1(\zeta, \xi)|$ as predicted by NLSE

$$\gamma_v = \frac{2}{\tau_2}, \ \omega_v = \sqrt{\frac{\tau_1^2 + \tau_2^2}{\tau_1^2 \tau_2^2}}, \ \tau_1 = 12.2 fs, \ \tau_2 = 32.0 fs.$$

The physical domain is $\Omega_0 = [0, 38\mu m] \times [-3\mu m, 3\mu m]$. On the left boundary x = 0, a hard source is injected, namely, by assigning the following time-dependent function to the magnetic field H_z ,

$$H_z(x = 0, y, t) = H_0 \sin(\omega_c t) \operatorname{sech}(y/w), \tag{48}$$

where, $\omega_c = 4.35 \times 10^{15}$ rad/s is the carrier frequency. And w, H_0 are the width and the magnitude of the incident wave, respectively, which will be specified later.

In order to facilitate the understanding of this set of numerical tests, let us first recall that in uniform glasses, the Maxwell's equations (47) with the nonlinear constitutive laws reduce to the nonlinear Schrödinger equation (NLSE) under paraxial assumption [14]. For the pulse given in (48), its propagation can be predicted by the solution of NLSE. In fact, the normalized NLSE

$$\begin{cases} i \frac{\partial u(\zeta,\xi)}{\partial \zeta} = \frac{1}{2} \frac{\partial^2 u(\zeta,\xi)}{\partial \xi^2} + |u(\zeta,\xi)|^2 u(\zeta,\xi), & \zeta \in (0,+\infty), \quad \xi \in (-\infty,+\infty), \\ u(0,\xi) = g(\xi), & \xi \in (-\infty,+\infty) \end{cases}$$
(49)

admits *bright soliton* solutions [7]. For example, if the boundary data is specified as $g_1(\xi) = \eta \operatorname{sech} \left(\eta(\xi - \xi_0) \right) e^{-i\Lambda \xi - i\phi}$, the classical solution of (49) is given by

$$u_1(\zeta,\xi) = \eta \operatorname{sech}\left(\eta(\xi - \xi_0 - \Lambda\zeta)\right) e^{-i\Lambda\xi - i\phi + i(\Lambda^2 - \eta^2)\zeta/2},\tag{50}$$

where η , ξ_0 , Λ , ϕ are the four basic soliton parameters. This special solution is called the fundamental soliton. In Fig. 2, we plot the profile of $|u_1(\zeta, \xi)|$ with $\eta = 1$, $\xi_0 = 0$, $\Lambda = 0$, $\phi = 0$. As one can see, the fundamental soliton propagates in the dispersive and weakly nonlinear medium without changing its amplitude, width or shape.

If the boundary data is prescribed as $g_2(\xi) = 2 \operatorname{sech}(\xi)$, with two identical pulses injected at $\zeta = 0$, then the following *second-order soliton* is generated

$$u_2(\zeta,\xi) = 4e^{-i\zeta/2} \frac{\cosh(3\xi) + 3e^{-i4\zeta}\cosh(\xi)}{\cosh(4\xi) + 4\cosh(2\xi) + 3\cos(4\zeta)}.$$
 (51)

This second-order soliton is the direct result of the interactions between the two fundamental solitons. As the phase difference between the two fundamental solitons varies from location



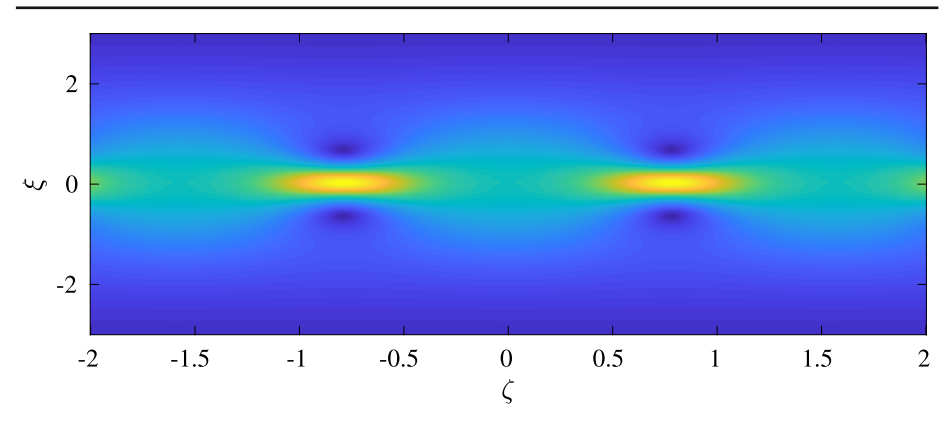


Fig. 3 Second-order soliton $|u_2(\zeta, \xi)|$ as predicted by NLSE

to location, their interference will lead to periodic variations in amplitude as depicted in Fig. 3.

In the following, we want to simulate these solitons using the Maxwell's equations (47) up to time $T = 300 \, f \, s$. Initially, all the fields are set to be zero. In our simulations, we only consider the DG schemes with Alternating I and Alternating II numerical fluxes, as both can naturally implement the boundary condition in (48) for H_z on the left boundary without the knowledge of the electric field E(x = 0, y, t). We refer the interested readers to [3] for numerical boundary treatments suitable for other alternating fluxes. With similarity, we will only present the simulation results by the Alternating I numerical flux.

To reduce the numerical artifacts from the remaining part of the domain boundary, we set the computational domain to be larger, i.e. $\Omega = [x_a, x_b] \times [y_a, y_b] = [0, 60\mu m] \times [-4\mu m, 4\mu m]$, and apply the following absorbing boundary conditions on the top, bottom and right boundaries, based on the characteristic decomposition of the linearized system as in [3] by neglecting the nonlinear effects and the delayed response in the constitutive relation.

• At $x = x_b$:

$$\left(\sqrt{\frac{\mu_0}{\epsilon_0 \epsilon_\infty}} H_{zh} + E_{yh}\right)_{x=x_b}^+ = \left(\sqrt{\frac{\mu_0}{\epsilon_0 \epsilon_\infty}} H_{zh} + E_{yh}\right)_{x=x_b}^-,
\left(\sqrt{\frac{\mu_0}{\epsilon_0 \epsilon_\infty}} H_{zh} - E_{yh}\right)_{x=x_b}^+ = 0;$$
(52)

• At $y = y_a$:

$$\left(\sqrt{\frac{\mu_0}{\epsilon_0 \epsilon_\infty}} H_{zh} + E_{xh}\right)_{y=y_a}^{-} = \left(\sqrt{\frac{\mu_0}{\epsilon_0 \epsilon_\infty}} H_{zh} + E_{xh}\right)_{y=y_a}^{+},
\left(\sqrt{\frac{\mu_0}{\epsilon_0 \epsilon_\infty}} H_{zh} - E_{xh}\right)_{y=y_a}^{-} = 0;$$
(53)

• At $y = y_b$:

$$\left(\sqrt{\frac{\mu_0}{\epsilon_0\epsilon_\infty}}H_{zh}-E_{xh}\right)_{y=y_b}^+ = \left(\sqrt{\frac{\mu_0}{\epsilon_0\epsilon_\infty}}H_{zh}-E_{xh}\right)_{y=y_b}^-,$$



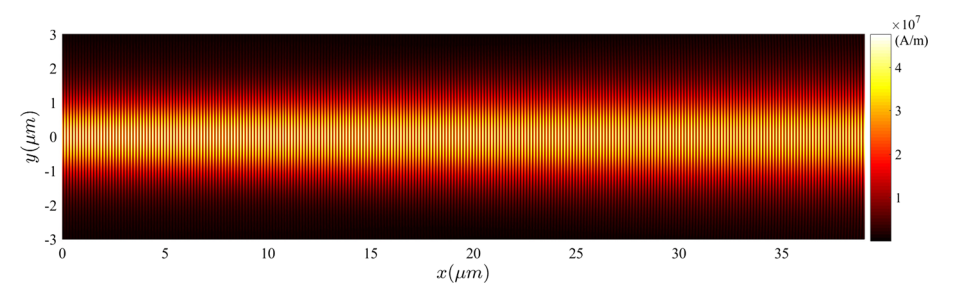


Fig. 4 Fundamental soliton propagation, snapshot of $|H_z|$ at t=T by Alternating I numerical flux. w=667.0 nm, $H_0=4.77\times10^7$ A/m

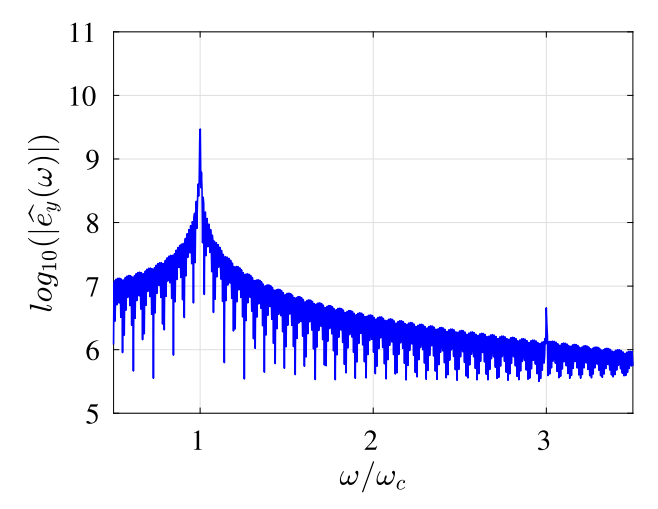


Fig. 5 Semi-log plot of the spectrum for fundamental soliton propagation

$$\left(\sqrt{\frac{\mu_0}{\epsilon_0 \epsilon_\infty}} H_{zh} + E_{xh}\right)_{y=y_h}^+ = 0. \tag{54}$$

We start with the fundamental soliton by setting w=667.0 nm, $H_0=4.77\times 10^7$ A/m in (48). In Fig. 4, we present a snapshot of the computed $|H_z|$ at t=T, and it shows that our simulated soliton maintains its width and amplitude quite well. We would also like to examine the high order harmonic generation in the soliton propagation. For this setup, since the third harmonic wave propagates along the polarization direction, we can integrate the E_y component to extract this information. In Fig. 5, we present the discrete Fourier transform $\widehat{e}_y(\omega)$ of $e_y(t) = \frac{\int_{y_0}^{y_0} E_{y_0}(x_r, y, t) dy}{y_0 - y_0}$, the average of E_y along y direction at $x_r = 50$ nm. One can observe that besides the signal with fundamental frequency ω_c , a third order harmonic signal is also detected.

Next we consider the propagation of second-order soliton by setting w=667.0 nm, $H_0=2\times4.77\times10^7$ A/m in (48). With this incident pulse, as predicted by the NLSE, two fundamental solitons will be launched to produce a second-order soliton, exhibiting periodic focusing and defocusing effect. This phenomenon is well reproduced by our schemes shown in Fig. 6. The corresponding spectrum for $e_y(t)$ in Fig. 7 shows that the third-order harmonic wave is also generated in this case.



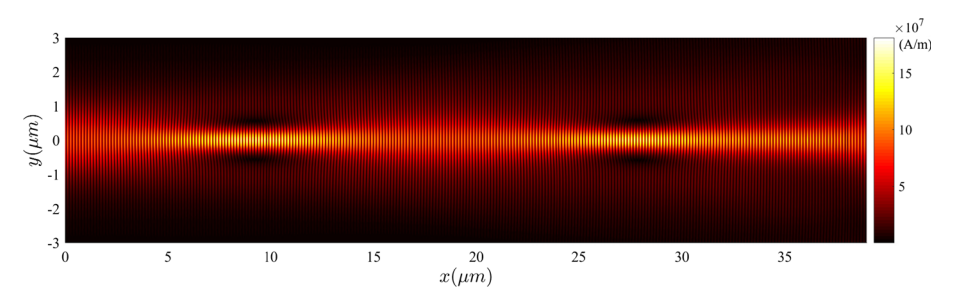


Fig. 6 Second-order soliton propagation, snapshot of $|H_z|$ at t=T by Alternating I numerical flux. w=667.0 nm, $H_0=2\times4.77\times10^7$ A/m

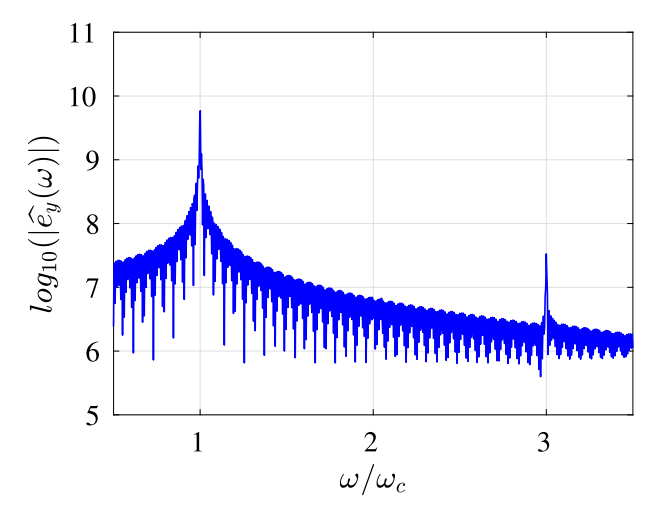


Fig. 7 Semi-log plot of the spectrum for second-order soliton propagation

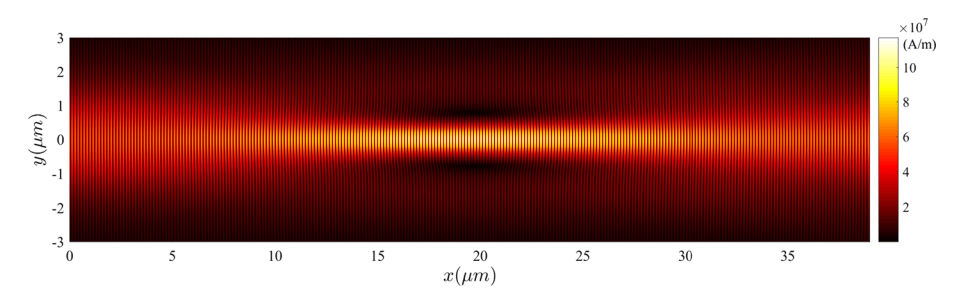


Fig. 8 Soliton propagation, snapshot of $|H_z|$ at t=T by Alternating I numerical flux. $w=r\times 667.0$ nm, $H_0=2/r\times 4.77\times 10^7$ A/m, r=5.99/3.99

If we further tune the parameters H_0 and w, both the width and amplitude of the soliton will change accordingly. Moreover, the period of the spatial focusing and defocusing in amplitude will diminish as the beam-width w decreases, see Figs. 8 and 9. The corresponding frequency domain information for e_y is shown in Fig. 10. These results are quite close to those reported in [14].



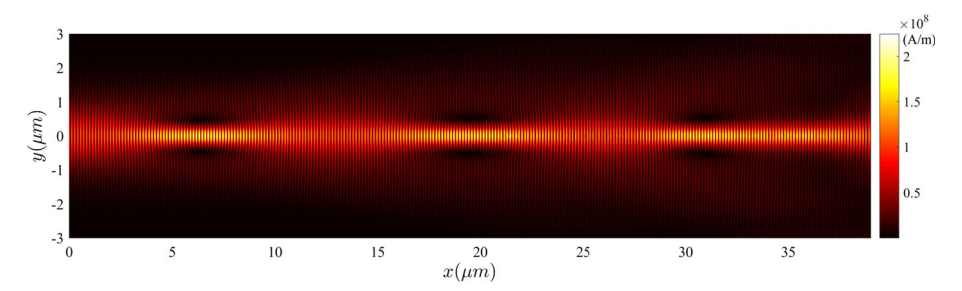


Fig. 9 Soliton propagation, snapshot of $|H_z|$ at t=T by Alternating I numerical flux. $w=r\times 667.0$ nm, $H_0=2/r\times 4.77\times 10^7$ A/m, r=3.26/3.99

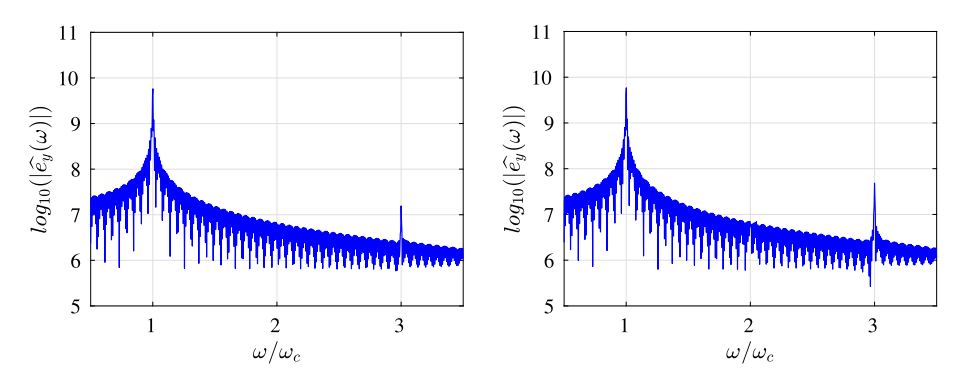


Fig. 10 Semi-log plot of the spectrum for soliton propagations. Left: r = 5.99/3.99, right: r = 3.26/3.99

3.2.2 Airhole Scattering

Next, we would like to simulate the scattering of a soliton by material discontinuities, in the form of an airhole sitting in a nonlinear glass. For this example, since the glasses are not uniform and the wave propagation is not paraxial, the full model of nonlinear Maxwell's equations is required to simulate the light-dielectric interactions [14]. The physical domain is $\Omega_0 = [0, 29\mu m] \times [-5\mu m, 5\mu m]$. Again, to reduce artificial boundary effects, the simulations are conducted in a larger computational domain $\Omega = [0, 32\mu m] \times [-12\mu m, 12\mu m]$, with approximated absorbing boundary conditions (52)–(54) applied on the top, bottom and right boundaries. On the left boundary, an incident wave (48) with $\omega_c = 4.35 \times 10^{15}$ rad/s, w = 667.0 nm, $H_0 = 2 \times 4.77 \times 10^7$ A/m is introduced. In the bulk of the optical media, there is a 250 nm \times 250 nm airhole with its center sitting at (5 μ m, 0). Modeling this airhole is realized by simply setting b = a = 0 in (47) in this region. All other model parameters are the same as in the previous example. We run the simulations to T = 160 f s. Again with visual similarity, only results by Alternating I numerical flux are presented.

In Fig. 11, we plot the magnetic field $|H_z|$ at time t = T. As is shown, the scattered wave does not totally escape but coalesces into a relatively weaker soliton after interacting with the airhole. This reformed soliton exhibits periodic focusing and defocusing effects again as in the previous example.

If the electromagnetic wave hits on a larger airhole of size 350 nm × 350 nm, the amount of scattering increases, see Fig. 12. Moreover, the refocusing effects gets weaker and happens at a longer distance away from the airhole. The numerical spectrum analysis in Fig. 13 reveals



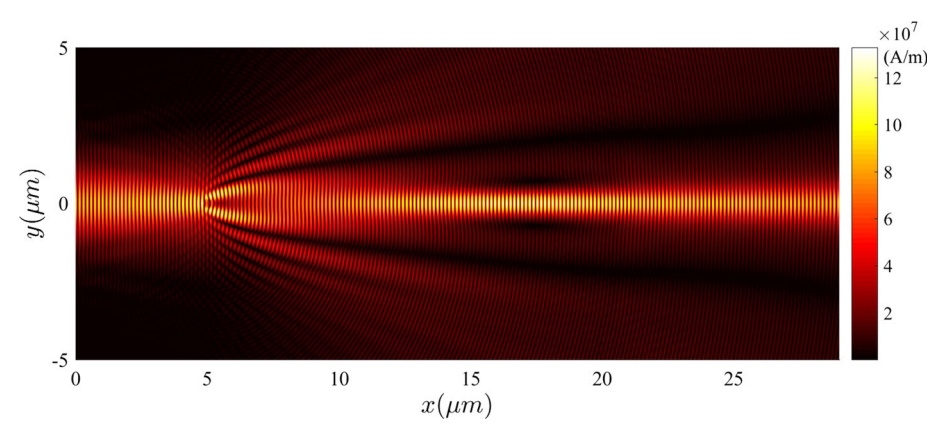


Fig. 11 Airhole scattering, snapshot of $|H_z|$ at t=T by Alternating I numerical flux. w=667.0 nm, $H_0=2\times4.77\times10^7\times$ A/m. Size: 250 nm \times 250 nm

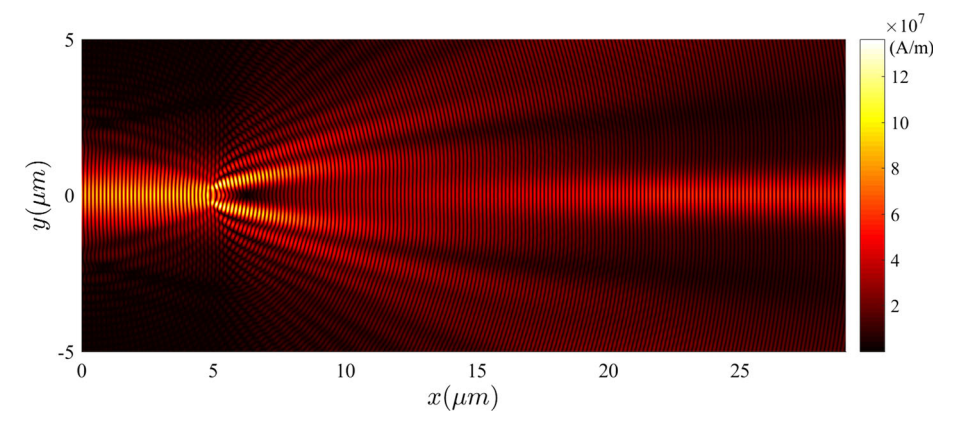


Fig. 12 Airhole scattering, snapshot of $|H_z|$ at t=T by Alternating I numerical flux. w=667.0 nm, $H_0=2\times4.77\times10^7\times$ A/m. Size: 350 nm \times 350 nm

that the third order harmonic wave is also generated in this airhole scattering. These results are in good agreement with the results in [14] by FDTD methods.

4 Conclusions

In this work, we extend the 1D energy stable DG schemes in [3] for nonlinear Maxwell's equations to multi-dimensions. Using a similar nonlinear treatment as in [3], we develop the leap-frog time scheme with provable energy stability for the model. The nodal DG methods are employed in space for the purpose of efficiency. Energy stability results are proved for semi- and fully-discrete schemes, and error estimates are established for the semi-discrete in space nodal DG methods. Several numerical examples in 2D are provided to demonstrate the performance of the proposed schemes. Robust and accurate numerical boundary treatments need to be investigated to further improve the efficiency in simulating nonlinear optical phenomena, along with their impact to numerical energy estimates (see [3] for such analysis).



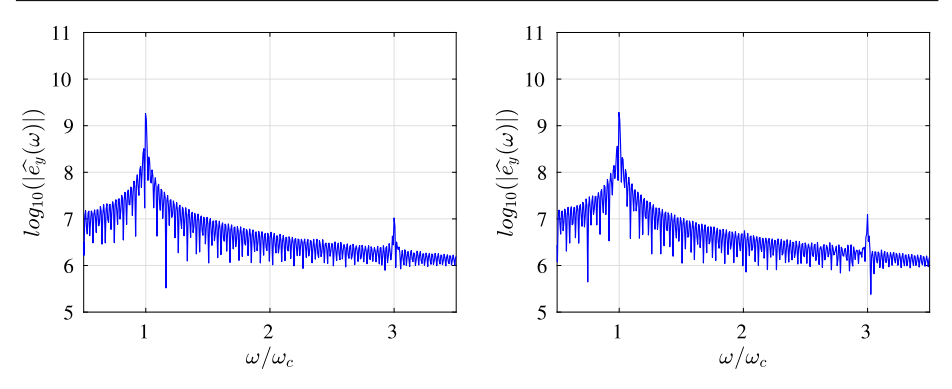


Fig. 13 Semi-log plots of the spectrum for airhole scattering. Left: $250 \text{ nm} \times 250 \text{ nm}$, Right: $350 \text{ nm} \times 350 \text{ nm}$

Computational efficiency can also be explored by utilizing the flexibility of DG methods in h, p-adaptive simulations.

Availability of data and materials The datasets generated and analyzed during the current study are available from the corresponding author on reasonable request (data transparency).

Declarations

Conflict of interest Financial interests: Author Lyu, Bokil and Cheng declare they have no financial interests. Author Li received an honorarium from University of Nevada Las Vegas as an invited speaker at the workshop Scientific Computing and Applications, held on March 6, 2021. Non-financial interests: Author Bokil serves as the Chair of the SIAM Career Opportunities Committee. Author Li serves on the SIAM Committee on Section Activities, on editorial boards of SIAM Journal on Numerical Analysis (2019—present), CSIAM Transaction on Applied Mathematics (2019—present), Applied Mathematics and Mechanics (English Edition) (2014—present). Author Li also served on the editorial board of SIAM Journal on Scientific Computing (2014—2019).

Code availability The code generated and analyzed during the current study is available from the corresponding author on reasonable request (software application or custom code).

Appendix A: Proof of Theorem 3

This section will be devoted to the proof of Theorem 3. We will start with some preparatory results on projection operators and their approximation properties, as well as inverse inequalities.

A.1 Preliminaries

We first consider the commonly used L^2 projection π_{xh} and Gauss-Radau projections π_{xh}^{\pm} onto $U_{xh}^k = \{u \in L^2([x_a, x_b]) : u|_{I_i} \in P^k(I_i), \ \forall i\}$ in the x direction on $[x_a, x_b]$. Here $P^k(I)$ consists of polynomials of degree up to k on an interval I.

1. L^2 projection π_{xh} : $L^2([x_a, x_b]) \to U_{xh}^k$, satisfying, $\forall i$, $\int_{x_{i-1}}^{x_{i+\frac{1}{2}}} (\pi_{xh} w)(x) v(x) dx = \int_{x_{i-1}}^{x_{i+\frac{1}{2}}} w(x) v(x) dx, \quad \forall v \in P^k(I_i);$



2. Gauss-Radau projection π_{xh}^+ : $H^1([x_a, x_b]) \to U_{xh}^k$, satisfying, $\forall i$,

$$\int_{x_{i-\frac{1}{2}}}^{x_{i+\frac{1}{2}}} (\pi_{xh}^+ w)(x) v(x) dx = \int_{x_{i-\frac{1}{2}}}^{x_{i+\frac{1}{2}}} w(x) v(x) dx, \quad \forall v \in P^{k-1}(I_i),$$

and

$$\left(\pi_{xh}^+ w\right) (x_{i-\frac{1}{2}}^+) = w(x_{i-\frac{1}{2}}^+);$$

3. Gauss-Radau projection π_{xh}^- : $H^1([x_a, x_b]) \to U_{xh}^k$, satisfying, $\forall i$,

$$\int_{x_{i-\frac{1}{2}}}^{x_{i+\frac{1}{2}}} (\pi_{xh}^- w)(x) v(x) dx = \int_{x_{i-\frac{1}{2}}}^{x_{i+\frac{1}{2}}} w(x) v(x) dx, \quad \forall v \in P^{k-1}(I_i),$$

and

$$\left(\pi_{xh}^- w\right)(x_{i+\frac{1}{2}}^-) = w(x_{i+\frac{1}{2}}^-).$$

The one-dimensional L^2 projection π_{yh} and Gauss-Radau projections π_{yh}^{\pm} can be defined similarly in the y direction onto $U_{yh}^k = \{u \in L^2([y_a, y_b]) : u|_{J_j} \in P^k(J_j), \forall j\}$. One can further define two-dimensional projection operators as tensor products of one-dimensional ones as follows [9,20].

1. $\Pi_h^{\pm,0} = \pi_{xh}^{\pm} \otimes \pi_{yh}$: $H^2(\Omega) \to V_h^k$, satisfying, $\forall v \in Q^k(K_{ij})$ and $\forall i, j,$

$$\int_{x_{i-\frac{1}{2}}}^{x_{i+\frac{1}{2}}} \int_{y_{j-\frac{1}{2}}}^{y_{j+\frac{1}{2}}} \left(\Pi_h^{\pm,0} w \right) (x,y) \frac{\partial v(x,y)}{\partial x} dx dy = \int_{x_{i-\frac{1}{2}}}^{x_{i+\frac{1}{2}}} \int_{y_{j-\frac{1}{2}}}^{y_{j+\frac{1}{2}}} w(x,y) \frac{\partial v(x,y)}{\partial x} dx dy$$

and

$$\int_{y_{j-\frac{1}{2}}}^{y_{j+\frac{1}{2}}} \left(\Pi_h^{\pm,0} w\right) (x_{i\mp\frac{1}{2}}^{\pm}, y) v(x_{i\mp\frac{1}{2}}^{\pm}, y) dy = \int_{y_{j-\frac{1}{2}}}^{y_{j+\frac{1}{2}}} w(x_{i\mp\frac{1}{2}}^{\pm}, y) v(x_{i\mp\frac{1}{2}}^{\pm}, y) dy;$$

2. $\Pi_h^{0,\pm} = \pi_{xh} \otimes \pi_{yh}^{\pm} \colon H^2(\Omega) \to V_h^k$, satisfying, $\forall v \in Q^k(K_{ij})$ and $\forall i, j$,

$$\int_{x_{i-\frac{1}{2}}}^{x_{i+\frac{1}{2}}} \int_{y_{j-\frac{1}{2}}}^{y_{j+\frac{1}{2}}} \left(\Pi_h^{0,\pm} w\right)(x,y) \frac{\partial v(x,y)}{\partial y} dx dy = \int_{x_{i-\frac{1}{2}}}^{x_{i+\frac{1}{2}}} \int_{y_{j-\frac{1}{2}}}^{y_{j+\frac{1}{2}}} w(x,y) \frac{\partial v(x,y)}{\partial y} dx dy$$

and

$$\int_{x_{i-\frac{1}{2}}}^{x_{i+\frac{1}{2}}} \Big(\Pi_h^{0,\pm}w\Big)(x,y_{j\mp\frac{1}{2}}^\pm)v(x,y_{j\mp\frac{1}{2}}^\pm)dx = \int_{x_{i-\frac{1}{2}}}^{x_{i+\frac{1}{2}}} w(x,y_{j\mp\frac{1}{2}}^\pm)v(x,y_{j\mp\frac{1}{2}}^\pm)dx;$$

3. $\Pi_h^{\pm,\pm} = \pi_{xh}^{\pm} \otimes \pi_{vh}^{\pm}$: $H^2(\Omega) \to V_h^k$, satisfying, $\forall v \in Q^{k-1}(K_{ij})$ and $\forall i, j,$

$$\begin{split} &\int_{x_{i-\frac{1}{2}}}^{x_{i+\frac{1}{2}}} \int_{y_{j-\frac{1}{2}}}^{y_{j+\frac{1}{2}}} \left(\Pi_h^{\pm,\pm}w\right)(x,y)v(x,y)dxdy = \int_{x_{i-\frac{1}{2}}}^{x_{i+\frac{1}{2}}} \int_{y_{j-\frac{1}{2}}}^{y_{j+\frac{1}{2}}} w(x,y)v(x,y)dxdy, \\ &\int_{x_{i-\frac{1}{2}}}^{x_{i+\frac{1}{2}}} \left(\Pi_h^{\pm,\pm}w\right)(x,y_{j\mp\frac{1}{2}}^{\pm})v(x,y_{j\mp\frac{1}{2}}^{\pm})dx = \int_{x_{i-\frac{1}{2}}}^{x_{i+\frac{1}{2}}} w(x,y_{j\mp\frac{1}{2}}^{\pm})v(x,y_{j\mp\frac{1}{2}}^{\pm})dx, \\ &\int_{y_{j-\frac{1}{2}}}^{y_{j+\frac{1}{2}}} \left(\Pi_h^{\pm,\pm}w\right)(x_{i\mp\frac{1}{2}}^{\pm},y)v(x_{i\mp\frac{1}{2}}^{\pm},y)dy = \int_{y_{j-\frac{1}{2}}}^{y_{j+\frac{1}{2}}} w(x_{i\mp\frac{1}{2}}^{\pm},y)v(x_{i\mp\frac{1}{2}}^{\pm},y)dy \end{split}$$



45

and

$$\left(\Pi_h^{\pm,\pm}w\right)(x_{i\mp\frac{1}{2}}^{\pm},y_{j\mp\frac{1}{2}}^{\pm}) = w(x_{i\mp\frac{1}{2}}^{\pm},y_{j\mp\frac{1}{2}}^{\pm});$$

4.) $\Pi_h^{0,0} = \pi_{xh} \otimes \pi_{yh}$: $L^2(\Omega) \to V_h^k$, satisfying, $\forall v \in Q^k(K_{ij})$ and $\forall i, j,$

$$\int_{x_{i-\frac{1}{2}}}^{x_{i+\frac{1}{2}}} \int_{y_{j-\frac{1}{2}}}^{y_{j+\frac{1}{2}}} \left(\Pi_h^{0,0} w\right)(x,y) v(x,y) dx dy = \int_{x_{i-\frac{1}{2}}}^{x_{i+\frac{1}{2}}} \int_{y_{j-\frac{1}{2}}}^{y_{j+\frac{1}{2}}} w(x,y) v(x,y) dx dy.$$

The following approximation results are standard for the analysis of DG methods, and can be established following classical arguments [8].

Lemma A1 (Approximation properties) Let \mathcal{P}_h be either the interpolation operator \mathcal{I}_h , or any of the projection operators $\Pi_h^{\pm,0}$, $\Pi_h^{0,\pm}$, $\Pi_h^{\pm,\pm}$, $\Pi_h^{0,0}$. There exist constants C_\star and C_k , such that $\forall w \in H^{k+1}(\Omega)$, there hold

$$\|w - \mathcal{P}_h w\|_{L^2(K)}^2 + h\|w - \mathcal{P}_h w\|_{L^2(\partial K)}^2 \le C_{\star} h^{2k+2} \|w\|_{H^{k+1}(K)}^2, \ \forall K \in \mathcal{T}_h$$
 (A1)

and

$$\|\mathcal{P}_h w\|_{\infty} \le C_k \|w\|_{\infty}. \tag{A2}$$

As a direct consequence of (A2), there holds

$$\|w - \mathcal{P}_h w\|_{\infty} \le C_k \|w\|_{\infty}. \tag{A3}$$

Associated with terms in our methods involving the interpolation operator to deal with nonlinearity more efficiently, it is convenient to work with a discrete norm $\|\cdot\|_h$ on V_h^k , which is equivalent to the standard L^2 norm.

Lemma A2 (Norm equivalence [10]) Define

$$\|v\|_h = \left(\sum_{i=1}^{N_x} \sum_{j=1}^{N_y} \sum_{m,n=0}^k \left| v(x_{im}, y_{jn}) \right|^2 \Delta x_i \Delta y_j \right)^{1/2},$$

then $\|\cdot\|_h$ is a norm on V_h^k . In addition, there exist constants C_{\star} , $\widetilde{C}_{\star} > 0$, such that

$$\widetilde{C}_{\star} \|v\|_h \leq \|v\| \leq C_{\star} \|v\|_h, \quad \forall v \in V_h^k.$$

Below are some immediate results of Lemma A2.

Lemma A3 There exists a constant C_{\star} , such that

$$\left| \int_{\Omega} \mathcal{I}_h(fg) d\Omega \right| \le C_{\star} \|f\| \|g\|, \quad \forall f, g \in W_h(\Omega). \tag{A4}$$

Proof By the definition of \mathcal{I}_h , and the exactness of (k+1)-point Gaussian-Legendre quadrature rule, the boundedness of $\{\widehat{\omega}_m\}_{m=0}^k$, Cauchy-Schwartz inequality, and norm equivalence in Lemma A2, we have

$$\left| \int_{\Omega} \mathcal{I}_{h}(fg) d\Omega \right| = \left| \sum_{i=1}^{N_{x}} \sum_{j=1}^{N_{y}} \frac{\Delta x_{i}}{2} \frac{\Delta y_{j}}{2} \sum_{m,n=0}^{k} \widehat{\omega}_{m} \widehat{\omega}_{n} f(x_{im}, y_{jn}) g(x_{im}, y_{jn}) \right|$$

$$\leq C_{k} \|f\|_{h} \|g\|_{h} \leq C_{\star} \|f\| \|g\|.$$



Finally, our analysis will need some inverse inequality [8].

Lemma A4 (Inverse inequality) There exists a constant C_{\star} , such that

$$h^{2} \|\nabla v\|_{L^{2}(K)}^{2} + h \|v\|_{L^{2}(\partial K)}^{2} \le C_{\star} \|v\|_{L^{2}(K)}^{2}, \quad \forall v \in V_{h}^{k}, \ \forall K \in \mathcal{T}_{h}. \tag{A5}$$

A.2 Proof of Theorem 3

Proof The proof will proceed similarly as that in [3]. The DG methods in [3] are of the modal form and for the 1D version of model (1). One difference in our analysis here comes from the use of the interpolation operator \mathcal{I}_h in the nodal DG setting to deal with nonlinear terms. Being two-dimensional also adds complexity to the use of projection operators in the proof.

For any component u of the solution (such as H_z , E_x , E_y etc), we first decompose its error as $u - u_h = (u - \mathcal{P}_h^u u) - (u_h - \mathcal{P}_h^u u) = \eta_u - \xi_u$, where the projection \mathcal{P}_h^u is taken to be $\Pi_h^{0,0}$ except for $\mathcal{P}_h^{E_x}$, $\mathcal{P}_h^{E_y}$, $\mathcal{P}_h^{H_z}$ when the numerical fluxes are alternating. When alternating fluxes are used, without loss of generality, we only consider one of the four possible cases, particularly, we consider Alternating I, given by (28) with $\dagger = +, \ddagger = -, \ddagger = +, \ddagger = -,$ and take

$$\mathcal{P}_h^{E_x} = \Pi_h^{0,+}, \ \mathcal{P}_h^{E_y} = \Pi_h^{+,0}, \ \mathcal{P}_h^{H_z} = \Pi_h^{-,-}.$$

We initialize the method by setting $\xi_u = u_h - \mathcal{P}_h^u u = 0$ at t = 0 for all solution components. **Step 1:** With the consistency of numerical fluxes, from (25), we can obtain the error equations:

$$\mu_0(\partial_t \eta_{H_z}, \phi) + \mathcal{B}_h^E(\eta_{E_x}, \eta_{E_y}, \phi) = \mu_0(\partial_t \xi_{H_z}, \phi) + \mathcal{B}_h^E(\xi_{E_x}, \xi_{E_y}, \phi), \quad \forall \phi \in V_h^k, \text{ (A6a)}$$

$$\left(\partial_t (D_x - D_{xh}), \phi\right) + \mathcal{B}_{xh}^H(\eta_{H_z}, \phi) = \mathcal{B}_{xh}^H(\xi_{H_z}, \phi), \quad \forall \phi \in V_h^k, \tag{A6b}$$

$$\left(\partial_t(D_y - D_{yh}), \phi\right) + \mathcal{B}_{yh}^H(\eta_{H_z}, \phi) = \mathcal{B}_{yh}^H(\xi_{H_z}, \phi), \quad \forall \phi \in V_h^k, \tag{A6c}$$

$$\partial_t \eta_P - \eta_I = \partial_t \xi_P - \xi_I, \tag{A6d}$$

$$\partial_t \boldsymbol{\eta}_J + \gamma \boldsymbol{\eta}_J + \omega_0^2 \boldsymbol{\eta}_P - \omega_p^2 \boldsymbol{\eta}_E = \partial_t \boldsymbol{\xi}_J + \gamma \boldsymbol{\xi}_J + \omega_0^2 \boldsymbol{\xi}_P - \omega_p^2 \boldsymbol{\xi}_E, \tag{A6e}$$

 $\partial_t \eta_O - \eta_\sigma = \partial_t \xi_O - \xi_\sigma,$

$$\partial_t \eta_\sigma + \gamma_v \eta_\sigma + \omega_v^2 \eta_Q - \partial_t \xi_\sigma - \gamma_v \xi_\sigma - \omega_v^2 \xi_Q = \omega_v^2 \left(|\boldsymbol{E}|^2 - \mathcal{I}_h \left(|\boldsymbol{E}_h|^2 \right) \right) \tag{A6f}$$

$$=\omega_v^2\left(|E|^2 - \mathcal{I}_h\left(|E|^2\right)\right) + \omega_v^2 \mathcal{I}_h\left(|E|^2 - |E_h|^2\right),\tag{A6g}$$

along with

$$\mathbf{D} - \mathbf{D}_{h} = \epsilon_{0} \epsilon_{\infty} (\eta_{E} - \xi_{E}) + \epsilon_{0} (\eta_{P} - \xi_{P}) + \epsilon_{0} a (1 - \theta) \left(|E|^{2} E - \mathcal{I}_{h} \left(|E_{h}|^{2} E_{h} \right) \right) + \epsilon_{0} a \theta (OE - \mathcal{I}_{h} (O_{h} E_{h})).$$
(A7)

Note that $\mathcal{P}_h^{\pmb{P}}=\mathcal{P}_h^{\pmb{J}}=\Pi_h^{0,0}$, then the equation (1d) implies

$$\partial_t \boldsymbol{\eta}_P - \boldsymbol{\eta}_I = \mathbf{0}. \tag{A8}$$

Therefore (A6d) further gives

$$\partial_t \boldsymbol{\xi}_P - \boldsymbol{\xi}_I = \mathbf{0}. \tag{A9}$$

Similarly, (A6f) gives

$$\partial_t \xi_O - \xi_\sigma = 0. \tag{A10}$$

Recall that the choice of \mathcal{P}_h^E depends on the numerical fluxes, then the equation (1e) implies $\partial_t \eta_J + \gamma \eta_J + \omega_0^2 \eta_P - \omega_p^2 (E - \Pi_h^{0,0} E) = 0$, this together with (A6e) leads to

$$\partial_t \boldsymbol{\xi}_J + \gamma \boldsymbol{\xi}_J + \omega_0^2 \boldsymbol{\xi}_P - \omega_p^2 \boldsymbol{\xi}_E = \omega_p^2 \mho_E, \tag{A11}$$

where

$$\mho_E = (E - \Pi_h^{0,0} E) - \eta_E = \begin{cases} \mathbf{0} & \text{central flux for } E \\ \Pi_h^E E - \Pi_h^{0,0} E & \text{alternating flux for } E \end{cases} . \tag{A12}$$

Step 2: Take $\phi = \xi_{H_z}$ in (A6a), $\phi = \xi_{E_x}$ in (A6b), and $\phi = \xi_{E_y}$ in (A6c), sum them up and use (30), we have,

$$\frac{\mu_0}{2} \frac{d}{dt} \| \xi_{H_z} \|^2 - \mu_0(\partial_t \eta_{H_z}, \xi_{H_z}) - \mathcal{B}_h^E(\eta_{E_x}, \eta_{E_y}, \xi_{H_z}) - \mathcal{B}_{xh}^H(\eta_{H_z}, \xi_{E_x}) - \mathcal{B}_{yh}^H(\eta_{H_z}, \xi_{E_y}) \\
= \left(\partial_t (\mathbf{D} - \mathbf{D}_h), \xi_E \right). \tag{A13}$$

Differentiate (A7) with respect to time t, and use that ∂_t and \mathcal{I}_h commute, we have

$$\left(\partial_{t}(\mathbf{D} - \mathbf{D}_{h}), \boldsymbol{\xi}_{E}\right) = \epsilon_{0} \epsilon_{\infty} \left(\partial_{t}(\boldsymbol{\eta}_{E} - \boldsymbol{\xi}_{E}), \boldsymbol{\xi}_{E}\right) + \epsilon_{0} \left(\partial_{t}(\boldsymbol{\eta}_{P} - \boldsymbol{\xi}_{P}), \boldsymbol{\xi}_{E}\right) \\
+ \epsilon_{0} a(1 - \theta) \left(\partial_{t}(|E|^{2}E) - \mathcal{I}_{h} \left(\partial_{t}(|E|^{2}E)\right), \boldsymbol{\xi}_{E}\right) \\
+ \epsilon_{0} a(1 - \theta) \left(\mathcal{I}_{h} \partial_{t} \left(|E|^{2}E - |E_{h}|^{2}E_{h}\right), \boldsymbol{\xi}_{E}\right) \\
+ \epsilon_{0} a\theta \left(\partial_{t}(QE) - \mathcal{I}_{h} \left(\partial_{t}(QE)\right), \boldsymbol{\xi}_{E}\right) + \epsilon_{0} a\theta \left(\mathcal{I}_{h} \partial_{t} \left(QE - Q_{h}E_{h}\right), \boldsymbol{\xi}_{E}\right).$$
(A14)

In next few steps, we will work with the terms on the right side of (A14) based on the error equations.

Step 2.1: the fourth term in (A14). Using $E_h = E - \eta_E + \xi_E$ and some direct manipulation, one can get

$$\partial_{t}\left(|\mathbf{E}|^{2}\mathbf{E} - |\mathbf{E}_{h}|^{2}\mathbf{E}_{h}\right) \cdot \boldsymbol{\xi}_{E} \\
= \partial_{t}\left(|\mathbf{E}|^{2}\mathbf{E}\right) \cdot \boldsymbol{\xi}_{E} - 2(\mathbf{E}_{h} \cdot \partial_{t}\mathbf{E}_{h})(\mathbf{E}_{h} \cdot \boldsymbol{\xi}_{E}) - |\mathbf{E}_{h}|^{2}\partial_{t}\mathbf{E}_{h} \cdot \boldsymbol{\xi}_{E} \\
= -\frac{3}{4}\partial_{t}\left(|\boldsymbol{\xi}_{E}|^{4}\right) - 2\partial_{t}\left(|\boldsymbol{\xi}_{E}|^{2}(\mathbf{E} - \boldsymbol{\eta}_{E}) \cdot \boldsymbol{\xi}_{E}\right) \\
- \partial_{t}\left(((\mathbf{E} - \boldsymbol{\eta}_{E}) \cdot \boldsymbol{\xi}_{E})^{2}\right) - \frac{1}{2}\partial_{t}\left(|\mathbf{E} - \boldsymbol{\eta}_{E}|^{2}|\boldsymbol{\xi}_{E}|^{2}\right) \\
- \frac{1}{2}\partial_{t}\left(|\mathbf{E} - \boldsymbol{\eta}_{E}|^{2}\right)|\boldsymbol{\xi}_{E}|^{2} - 2\left((\mathbf{E} - \boldsymbol{\eta}_{E}) \cdot \boldsymbol{\xi}_{E}\right)\left(\partial_{t}(\mathbf{E} - \boldsymbol{\eta}_{E}) \cdot \boldsymbol{\xi}_{E}\right) \\
- |\boldsymbol{\xi}_{E}|^{2}\left(\partial_{t}(\mathbf{E} - \boldsymbol{\eta}_{E}) \cdot \boldsymbol{\xi}_{E}\right) \\
- |\mathbf{E} - \boldsymbol{\eta}_{E}|^{2}\left(\partial_{t}(\mathbf{E} - \boldsymbol{\eta}_{E}) \cdot \boldsymbol{\xi}_{E}\right) - \partial_{t}\left(|\mathbf{E} - \boldsymbol{\eta}_{E}|^{2}\right)\left((\mathbf{E} - \boldsymbol{\eta}_{E}) \cdot \boldsymbol{\xi}_{E}\right) \\
+ \partial_{t}\left(|\mathbf{E}|^{2}\mathbf{E}\right) \cdot \boldsymbol{\xi}_{E}. \tag{A15}$$



And the last three terms in (A15) can be further written as

$$-\partial_t \left(|E - \eta_E|^2 (E - \eta_E) - |E|^2 E \right) \cdot \xi_E$$

$$= \partial_t \left(|\eta_E|^2 \eta_E - |\eta_E|^2 E - 2(E \cdot \eta_E) \eta_E + 2(E \cdot \eta_E) E + |E|^2 \eta_E \right) \cdot \xi_E. \tag{A16}$$

With (A16) and (A15), and Lemma 1, we now have

$$\begin{split}
&\left(\mathcal{I}_{h}\partial_{t}(|E|^{2}E - |E_{h}|^{2}E_{h}), \xi_{E}\right) = \int_{\Omega} \mathcal{I}_{h}\left(\partial_{t}(|E|^{2}E - |E_{h}|^{2}E_{h}) \cdot \xi_{E}\right) d\Omega \\
&= -\frac{3}{4}\frac{d}{dt} \int_{\Omega} \mathcal{I}_{h}\left(|\xi_{E}|^{4}\right) d\Omega - 2\frac{d}{dt} \int_{\Omega} \mathcal{I}_{h}\left(|\xi_{E}|^{2}(E - \eta_{E}) \cdot \xi_{E}\right) d\Omega \\
&- \frac{d}{dt} \int_{\Omega} \mathcal{I}_{h}((E - \eta_{E}) \cdot \xi_{E})^{2} d\Omega \\
&- \frac{1}{2}\frac{d}{dt} \int_{\Omega} \mathcal{I}_{h}\left(|E - \eta_{E}|^{2}|\xi_{E}|^{2}\right) d\Omega - \frac{1}{2} \int_{\Omega} \mathcal{I}_{h}\left(\partial_{t}(|E - \eta_{E})|^{2})|\xi_{E}|^{2}\right) d\Omega \\
&- 2 \int_{\Omega} \mathcal{I}_{h}\left(((E - \eta_{E}) \cdot \xi_{E})(\partial_{t}(E - \eta_{E}) \cdot \xi_{E})) d\Omega \\
&- \int_{\Omega} \mathcal{I}_{h}\left(|\xi_{E}|^{2}(\partial_{t}(E - \eta_{E}) \cdot \xi_{E})\right) d\Omega \\
&+ \int_{\Omega} \mathcal{I}_{h}\left(\partial_{t}(|\eta_{E}|^{2}\eta_{E} - |\eta_{E}|^{2}E - 2(E \cdot \eta_{E})\eta_{E} \\
&+ 2(E \cdot \eta_{E})E + |E|^{2}\eta_{E}\right) \cdot \xi_{E}\right) d\Omega.
\end{split} \tag{A17}$$

Step 2.2: the sixth term in (A14). We consider

$$\partial_{t}(QE - Q_{h}E_{h}) \cdot \boldsymbol{\xi}_{E} = \partial_{t} \left(QE - (Q - \eta_{Q} + \boldsymbol{\xi}_{Q})(E - \eta_{E} + \boldsymbol{\xi}_{E}) \right) \cdot \boldsymbol{\xi}_{E}
= \partial_{t} \left(Q\eta_{E} + \eta_{Q}(E - \eta_{E}) \right) \cdot \boldsymbol{\xi}_{E} - \frac{1}{2} \partial_{t} (Q - \eta_{Q}) |\boldsymbol{\xi}_{E}|^{2}
- \frac{1}{2} \partial_{t} \left((Q - \eta_{Q}) |\boldsymbol{\xi}_{E}|^{2} \right) - \partial_{t} \boldsymbol{\xi}_{Q} (E - \eta_{E}) \cdot \boldsymbol{\xi}_{E}
- \boldsymbol{\xi}_{Q} \partial_{t} (E - \eta_{E}) \cdot \boldsymbol{\xi}_{E} - \frac{1}{2} \partial_{t} \boldsymbol{\xi}_{Q} |\boldsymbol{\xi}_{E}|^{2} - \frac{1}{2} \partial_{t} \left(\boldsymbol{\xi}_{Q} |\boldsymbol{\xi}_{E}|^{2} \right). \quad (A18)$$

Observe that

$$(|E|^{2} - |E_{h}|^{2})\xi_{\sigma} = (|E|^{2} - |E - \eta_{E} + \xi_{E}|^{2})\xi_{\sigma}$$

$$= (|E|^{2} - |E - \eta_{E}|^{2} - 2(E - \eta_{E}) \cdot \xi_{E} - |\xi_{E}|^{2})\xi_{\sigma}$$

$$= (2E \cdot \eta_{E} - |\eta_{E}|^{2} - 2(E - \eta_{E}) \cdot \xi_{E})\xi_{\sigma} - \partial_{t}\xi_{Q}|\xi_{E}|^{2}, \quad (A19)$$

where we have used (A10) in the last equality. With (A19), (A10) and (A6g), and Lemma 1, we have

$$\begin{split} & \int_{\Omega} \mathcal{I}_h \left(\partial_t \xi_{\mathcal{Q}} | \boldsymbol{\xi}_{\boldsymbol{E}} |^2 \right) d\Omega \\ & = - \int_{\Omega} \mathcal{I}_h \left(|\boldsymbol{E}|^2 - |\boldsymbol{E}_h|^2 \right) \xi_{\sigma} d\Omega \\ & + \int_{\Omega} \mathcal{I}_h \Big((2\boldsymbol{E} \cdot \boldsymbol{\eta}_{\boldsymbol{E}} - |\boldsymbol{\eta}_{\boldsymbol{E}}|^2 - 2(\boldsymbol{E} - \boldsymbol{\eta}_{\boldsymbol{E}}) \cdot \boldsymbol{\xi}_{\boldsymbol{E}}) \xi_{\sigma} \Big) d\Omega \end{split}$$



$$= \int_{\Omega} (|\mathbf{E}|^{2} - \mathcal{I}_{h} (|\mathbf{E}|^{2})) \, \xi_{\sigma} d\Omega$$

$$+ \int_{\Omega} \mathcal{I}_{h} \Big((2\mathbf{E} \cdot \boldsymbol{\eta}_{E} - |\boldsymbol{\eta}_{E}|^{2} - 2(\mathbf{E} - \boldsymbol{\eta}_{E}) \cdot \boldsymbol{\xi}_{E}) \xi_{\sigma} \Big) d\Omega$$

$$- \frac{1}{\omega_{v}^{2}} \int_{\Omega} (\partial_{t} \eta_{\sigma} + \gamma_{v} \eta_{\sigma} + \omega_{v}^{2} \eta_{Q}) \, \xi_{\sigma} d\Omega$$

$$+ \frac{1}{2\omega_{v}^{2}} \frac{d}{dt} \int_{\Omega} \xi_{\sigma}^{2} d\Omega + \frac{\gamma_{v}}{\omega_{v}^{2}} \int_{\Omega} \xi_{\sigma}^{2} d\Omega + \frac{1}{2} \frac{d}{dt} \int_{\Omega} \xi_{Q}^{2} d\Omega. \tag{A20}$$

Combine (A18) and (A20), and use Lemma 1, we have

$$\begin{split} &\left(\mathcal{I}_{h}\partial_{t}\left(QE-Q_{h}E_{h}\right),\boldsymbol{\xi}_{E}\right)=\int_{\Omega}\mathcal{I}_{h}\left(\partial_{t}(QE-Q_{h}E_{h})\cdot\boldsymbol{\xi}_{E}\right)d\Omega\\ &=-\frac{d}{dt}\int_{\Omega}\left(\frac{1}{2}\mathcal{I}_{h}\left((Q-\eta_{Q})|\boldsymbol{\xi}_{E}|^{2}\right)+\frac{1}{2}\mathcal{I}_{h}\left(\boldsymbol{\xi}_{Q}|\boldsymbol{\xi}_{E}|^{2}\right)+\frac{1}{4\omega_{v}^{2}}\boldsymbol{\xi}_{\sigma}^{2}+\frac{1}{4}\boldsymbol{\xi}_{Q}^{2}\right)d\Omega\\ &-\frac{\gamma_{v}}{2\omega_{v}^{2}}\int_{\Omega}\boldsymbol{\xi}_{\sigma}^{2}d\Omega\\ &+\int_{\Omega}\mathcal{I}_{h}\left(\partial_{t}(Q\boldsymbol{\eta}_{E}+\eta_{Q}(E-\boldsymbol{\eta}_{E}))\cdot\boldsymbol{\xi}_{E}\right)d\Omega-\frac{1}{2}\int_{\Omega}\mathcal{I}_{h}\left(\partial_{t}(Q-\eta_{Q})|\boldsymbol{\xi}_{E}|^{2}\right)d\Omega\\ &-\int_{\Omega}\mathcal{I}_{h}\left(\boldsymbol{\xi}_{Q}\partial_{t}(E-\boldsymbol{\eta}_{E})\cdot\boldsymbol{\xi}_{E}\right)d\Omega-\frac{1}{2}\int_{\Omega}\mathcal{I}_{h}\left((2E\cdot\boldsymbol{\eta}_{E}-|\boldsymbol{\eta}_{E}|^{2})\boldsymbol{\xi}_{\sigma}\right)d\Omega\\ &+\frac{1}{2\omega_{v}^{2}}\int_{\Omega}\left(\partial_{t}\eta_{\sigma}+\gamma_{v}\eta_{\sigma}+\omega_{v}^{2}\eta_{Q})\boldsymbol{\xi}_{\sigma}d\Omega-\frac{1}{2}\int_{\Omega}\left(|E|^{2}-\mathcal{I}_{h}\left(|E|^{2}\right)\right)\boldsymbol{\xi}_{\sigma}d\Omega. \end{split} \tag{A21}$$

Here we have dropped the term $\int_{\Omega} \mathcal{I}_h \Big((\partial_t \xi_Q - \xi_\sigma) (E - \eta_E) \cdot \xi_E \Big) d\Omega$ due to (A10).

Step 2.3: the first and second terms in (A14). Use (A11), (A9), and (A8), we have

$$(\partial_{t}(\eta_{P} - \xi_{P}), \xi_{E})$$

$$= (\partial_{t}\eta_{P}, \xi_{E}) - \frac{1}{\omega_{p}^{2}} (\partial_{t}\xi_{P}, \partial_{t}\xi_{J} + \gamma\xi_{J} + \omega_{0}^{2}\xi_{P} - \omega_{p}^{2}\mho_{E})$$

$$= (\eta_{J}, \xi_{E}) + (\mho_{E}, \xi_{J}) - \frac{1}{2\omega_{p}^{2}} \frac{d}{dt} \int_{\Omega} |\xi_{J}|^{2} d\Omega$$

$$- \frac{\gamma}{\omega_{p}^{2}} \int_{\Omega} |\xi_{J}|^{2} d\Omega - \frac{\omega_{0}^{2}}{2\omega_{p}^{2}} \frac{d}{dt} \int_{\Omega} |\xi_{P}|^{2} d\Omega. \tag{A22}$$

In addition

$$(\partial_t(\eta_E - \xi_E), \xi_E) = (\partial_t \eta_E, \xi_E) - \frac{1}{2} \frac{d}{dt} \int_{\Omega} |\xi_E|^2 d\Omega. \tag{A23}$$

Now we can gather (A17), (A21)–(A23) for (A13)–(A14), and come up with the following identity,

$$\frac{d}{dt}\widehat{\mathcal{E}}_h + \frac{\epsilon_0 \gamma}{\omega_p^2} \int_{\Omega} |\xi_{\boldsymbol{J}}|^2 d\Omega + \frac{\epsilon_0 a \theta \gamma_v}{2\omega_v^2} \int_{\Omega} \xi_{\sigma}^2 d\Omega = \sum_{i=0}^4 \Lambda_i, \tag{A24}$$



where

$$\begin{split} \widehat{\mathcal{E}_h} &= \int_{\Omega} \left(\frac{\mu_0}{2} \xi_{H_z}^2 + \frac{\epsilon_0 \epsilon_\infty}{2} |\xi_E|^2 + \frac{\epsilon_0}{2\omega_p^2} |\xi_J|^2 + \frac{\epsilon_0 \omega_0^2}{2\omega_p^2} |\xi_P|^2 + \frac{\epsilon_0 a\theta}{4\omega_v^2} \xi_\sigma^2 \right) d\Omega \\ &+ \int_{\Omega} \mathcal{I}_h \left(\frac{\epsilon_0 a\theta}{2} \xi_Q |\xi_E|^2 + \frac{3\epsilon_0 a(1-\theta)}{4} |\xi_E|^4 + \frac{\epsilon_0 a\theta}{4} \xi_Q^2 \right) d\Omega \\ &+ \frac{\epsilon_0 a\theta}{2} \int_{\Omega} \mathcal{I}_h \left((Q - \eta_Q) |\xi_E|^2 \right) d\Omega \\ &+ \epsilon_0 a(1-\theta) \int_{\Omega} \mathcal{I}_h \left(2 |\xi_E|^2 (E - \eta_E) \cdot \xi_E + ((E - \eta_E) \cdot \xi_E)^2 + \frac{1}{2} |E - \eta_E|^2 |\xi_E|^2 \right) d\Omega, \\ \Lambda_0 &= \epsilon_0 a(1-\theta) \left(\partial_t (|E|^2 E) - \mathcal{I}_h \left(\partial_t (|E|^2 E) \right), \xi_E \right) + \epsilon_0 a\theta \left(\partial_t (QE) - \mathcal{I}_h \left(\partial_t (QE) \right), \xi_E \right) \\ &- \frac{\epsilon_0 a\theta}{2} \left(|E|^2 - \mathcal{I}_h (|E|^2), \xi_\sigma \right), \quad \Lambda_1 = \mu_0 (\partial_t \eta_{H_z}, \xi_{H_z}), \\ \Lambda_2 &= \mathcal{B}_h^E (\eta_{E_x}, \eta_{E_y}, \xi_{H_z}) + \mathcal{B}_{xh}^H (\eta_{H_z}, \xi_{E_x}) + \mathcal{B}_{yh}^H (\eta_{H_z}, \xi_{E_y}), \\ \Lambda_3 &= \frac{\epsilon_0 a\theta}{2\omega_v^2} (\partial_t \eta_\sigma + \gamma_v \eta_\sigma + \omega_v^2 \eta_Q, \xi_\sigma) - \frac{\epsilon_0 a\theta}{2} (\mathcal{I}_h (2E \cdot \eta_E - |\eta_E|^2), \xi_\sigma) \\ \Lambda_4 &= \epsilon_0 \epsilon_\infty (\partial_t \eta_E, \xi_E) + \epsilon_0 (\eta_J, \xi_E) + \epsilon_0 (\mho_E, \xi_J) - \epsilon_0 a\theta \int_{\Omega} \mathcal{I}_h \left(\xi_Q \partial_t (E - \eta_E) \cdot \xi_E \right) d\Omega \\ &- 2\epsilon_0 a(1-\theta) \int_{\Omega} \mathcal{I}_h \left(((E - \eta_E) \cdot \xi_E) (\partial_t (E - \eta_E) \cdot \xi_E) \right) d\Omega \\ &- \frac{\epsilon_0 a(1-\theta)}{2} \int_{\Omega} \mathcal{I}_h \left(\partial_t \left(|E - \eta_E|^2 \right) |\xi_E|^2 \right) d\Omega \\ &- \epsilon_0 a(1-\theta) \int_{\Omega} \mathcal{I}_h \left(|\xi_E|^2 \partial_t (E - \eta_E) \cdot \xi_E \right) d\Omega \\ &+ \epsilon_0 a\theta \int_{\Omega} \mathcal{I}_h \left(\partial_t (Q\eta_E + \eta_Q (E - \eta_E)) \cdot \xi_E \right) d\Omega \\ &- \frac{\epsilon_0 a\theta}{2} \int_{\Omega} \mathcal{I}_h \left(\partial_t (Q - \eta_Q) |\xi_E|^2 \right) d\Omega \\ &+ \epsilon_0 a(1-\theta) \int_{\Omega} \mathcal{I}_h \left(\partial_t (\eta_E |^2 \eta_E - |\eta_E|^2 E - 2(E \cdot \eta_E) \eta_E \right) \\ &+ \epsilon_0 a(1-\theta) \int_{\Omega} \mathcal{I}_h \left(\partial_t (\eta_E |^2 \eta_E - |\eta_E|^2 E - 2(E \cdot \eta_E) \eta_E \right) \\ &+ \epsilon_0 a(1-\theta) \int_{\Omega} \mathcal{I}_h \left(\partial_t (Q - \eta_Q) |\xi_E|^2 \right) d\Omega \\ &+ \epsilon_0 a(1-\theta) \int_{\Omega} \mathcal{I}_h \left(\partial_t (Q - \eta_Q) |\xi_E|^2 \right) d\Omega \\ &+ \epsilon_0 a(1-\theta) \int_{\Omega} \mathcal{I}_h \left(\partial_t (Q - \eta_Q) |\xi_E|^2 \right) d\Omega \\ &+ \epsilon_0 a(1-\theta) \int_{\Omega} \mathcal{I}_h \left(\partial_t (Q - \eta_Q) |\xi_E|^2 \right) d\Omega \\ &+ \epsilon_0 a(1-\theta) \int_{\Omega} \mathcal{I}_h \left(\partial_t (Q - \eta_Q) |\xi_E|^2 \right) d\Omega \\ &+ \epsilon_0 a(1-\theta) \int_{\Omega} \mathcal{I}_h \left(\partial_t (Q - \eta_Q) |\xi_E|^2 \right) d\Omega \\ &+ \epsilon_0 a(1-\theta) \int_{\Omega} \mathcal{I}_h \left(\partial_t (Q - \eta_Q) |\xi_E|^2 \right) d\Omega \\ &+ \epsilon_0 a(1-\theta) \int_{\Omega} \mathcal{I}_h \left(\partial_t (Q - \eta_Q) |\xi_E|^2 \right) d\Omega \\ &+ \epsilon_0 a(1-\theta) \int_{\Omega} \mathcal{I}_h \left(\partial_t (Q - \eta_Q) |\xi_E|^2 \right) d$$

Step 3: Next we will estimate terms on both sides of (A24).

Step 3.1: to estimate the left hand side of (A24). Let ρ_{err} , $\kappa_{err} \in (0, 1)$ be two arbitrary constants, then by Cauchy-Schwartz inequality, Lemmas 1-2, we have

$$\begin{split} \widehat{\mathcal{E}_h} &\geq \int_{\Omega} \left(\frac{\mu_0}{2} \xi_{H_z}^2 + \frac{\epsilon_0 \epsilon_\infty \kappa_{err}}{2} |\boldsymbol{\xi}_E|^2 + \frac{\epsilon_0}{2\omega_p^2} |\boldsymbol{\xi}_J|^2 + \frac{\epsilon_0 \omega_0^2}{2\omega_p^2} |\boldsymbol{\xi}_P|^2 + \frac{\epsilon_0 a \theta}{4\omega_v^2} \xi_\sigma^2 \right) d\Omega \\ &+ \int_{\Omega} \left(\frac{\epsilon_0 a (1-\theta) \rho_{err}}{12} \mathcal{I}_h \left(|\boldsymbol{\xi}_E|^4 \right) + \frac{\epsilon_0 a \theta \rho_{err}}{4} \xi_Q^2 \right) d\Omega \\ &+ \int_{\Omega} \mathcal{I}_h \left(\frac{\epsilon_0 a \theta}{2} \xi_Q |\boldsymbol{\xi}_E|^2 + \frac{\epsilon_0 a (1-\theta) (1-\rho_{err})}{12} |\boldsymbol{\xi}_E|^4 + \frac{\epsilon_0 a \theta (1-\rho_{err})}{4} \xi_Q^2 \right) d\Omega \end{split}$$



(2021) 89:45

$$+ \frac{\epsilon_0}{2} \int_{\Omega} \mathcal{I}_h \left(\left(\epsilon_{\infty} (1 - \kappa_{err}) + a\theta (Q - \eta_Q) \right) |\boldsymbol{\xi}_E|^2 \right) d\Omega$$

$$+ \frac{3\epsilon_0 a (1 - \theta)}{2} \int_{\Omega} \mathcal{I}_h \left(\left((\boldsymbol{E} - \boldsymbol{\eta}_E) \cdot \boldsymbol{\xi}_E + \frac{2}{3} |\boldsymbol{\xi}_E| \right)^2 \right) d\Omega \ge \mathcal{E}_h^{(mod)}, \tag{A25}$$

where

$$\begin{split} \mathcal{E}_{h}^{(mod)} &= \int_{\Omega} \left(\frac{\mu_{0}}{2} \xi_{H_{z}}^{2} + \frac{\epsilon_{0} \epsilon_{\infty} \kappa_{err}}{2} |\boldsymbol{\xi}_{E}|^{2} + \frac{\epsilon_{0}}{2 \omega_{p}^{2}} |\boldsymbol{\xi}_{J}|^{2} + \frac{\epsilon_{0} \omega_{0}^{2}}{2 \omega_{p}^{2}} |\boldsymbol{\xi}_{P}|^{2} \right) d\Omega \\ &+ \int_{\Omega} \left(\frac{\epsilon_{0} a \theta}{4 \omega_{v}^{2}} \xi_{\sigma}^{2} + \frac{\epsilon_{0} a (1 - \theta) \rho_{err}}{12} \mathcal{I}_{h} \left(|\boldsymbol{\xi}_{E}|^{4} \right) + \frac{\epsilon_{0} a \theta \rho_{err}}{4} \xi_{Q}^{2} \right) d\Omega. \end{split}$$

Here (24) in Lemma 2, as well as Conditions 1-2 in (39)–(40) have been used. In fact, by Condition 1, we have

$$\frac{\epsilon_0 a \theta}{2} \xi_Q |\xi_E|^2 + \frac{\epsilon_0 a (1-\theta) (1-\rho_{err})}{12} |\xi_E|^4 + \frac{\epsilon_0 a \theta (1-\rho_{err})}{4} \xi_Q^2 \geq 0,$$

while with Condition 2, there holds

$$\epsilon_{\infty}(1 - \kappa_{err}) + a\theta(Q - \eta_{Q}) \ge \epsilon_{\infty}(1 - \kappa_{err}) - a\theta \|\Pi_{h}^{0,0}Q\|_{\infty}$$

$$\ge \epsilon_{\infty}(1 - \kappa_{err}) - a\theta C_{k}\|Q\|_{\infty} \ge 0.$$

Step 3.2: to estimate Λ_0 and Λ_1 in (A24). For Λ_0 , we apply Cauchy-Schwartz inequality and the approximation properties in Lemma A1, and obtain

$$|\Lambda_0| \le CC(\kappa_{err})h^{2k+2} + \frac{\epsilon_0 \epsilon_\infty \kappa_{err}}{12} \|\boldsymbol{\xi}_E\|^2 + \frac{\epsilon_0 a\theta}{8\omega_v^2} \|\boldsymbol{\xi}_\sigma\|^2. \tag{A26}$$

For Λ_1 , with that ∂_t and $\mathcal{P}_h^{H_z}$ commute, and Lemma A1, we have

$$|\Lambda_1| \le \mu_0 \|\partial_t H_z - \mathcal{P}_h^{H_z} \partial_t H_z\|^2 + \frac{\mu_0}{4} \|\xi_{H_z}\|^2 \le Ch^{2k+2} + \frac{\mu_0}{4} \|\xi_{H_z}\|^2. \tag{A27}$$

Step 3.3: to estimate Λ_2 in (A24). For Λ_2 , when the central fluxes (27) are used, we have

$$|\Lambda_{2}| = \left| \sum_{i=1}^{N_{x}} \int_{y_{a}}^{y_{b}} \left(\widehat{\eta_{E_{y}}}(y) [\xi_{H_{z}}] + \widetilde{\eta_{H_{z}}}(y) [\xi_{E_{y}}] \right)_{x_{i+\frac{1}{2}}} dy - \sum_{j=1}^{N_{y}} \int_{x_{a}}^{x_{b}} \left(\widehat{\widehat{\eta_{E_{x}}}}(x) [\xi_{H_{z}}] + \widetilde{\eta_{H_{z}}}(x) [\xi_{E_{x}}] \right)_{y_{j+\frac{1}{2}}} dx \right| \\ \leq CC(\kappa_{err}) h^{2k} + \frac{\mu_{0}}{4} \|\xi_{H_{z}}\|^{2} + \frac{\epsilon_{0} \epsilon_{\infty} \kappa_{err}}{12} \|\xi_{E}\|^{2}.$$
(A28)

The inverse inequality in (A5) is applied. When the alternating fluxes (28) are used with $\dagger = +, \ddagger = -, \natural = +, \sharp = -$, there holds



$$|\Lambda_{2}| = \left| (\eta_{H_{z}}, \partial_{x} \xi_{E_{y}}) + \sum_{i=1}^{N_{x}} \int_{y_{a}}^{y_{b}} \widetilde{\eta_{H_{z}}}(y) [\xi_{E_{y}}]_{x_{i+\frac{1}{2}}} dy - (\eta_{H_{z}}, \partial_{y} \xi_{E_{x}}) \right.$$

$$\left. - \sum_{j=1}^{N_{y}} \int_{x_{a}}^{x_{b}} \widetilde{\eta_{H_{z}}}(x) [\xi_{E_{x}}]_{y_{j+\frac{1}{2}}} dx \right|$$

$$\leq CC(\kappa_{err}) h^{2k+2} + \frac{\epsilon_{0} \epsilon_{\infty} \kappa_{err}}{12} \|\xi_{E}\|^{2}. \tag{A29}$$

Here for the case of the alternating fluxes, we have used the super-convergence result established in [20] (see its Lemma 3.4) to gain the extra h^2 factor, and this is important for us to obtain the optimal error estimates.

Step 3.4: to estimate Λ_3 in (A24). For Λ_3 , we first bound the second term based on Lemma 1 and Lemma A3,

$$\left| \left(\mathcal{I}_h \left(2\boldsymbol{E} \cdot \boldsymbol{\eta}_E - |\boldsymbol{\eta}_E|^2 \right), \xi_{\sigma} \right) \right| = \left| \int_{\Omega} \mathcal{I}_h \left(\left(2\boldsymbol{E} \cdot \boldsymbol{\eta}_E - |\boldsymbol{\eta}_E|^2 \right) \xi_{\sigma} \right) d\Omega \right|$$

$$\leq C_{\star} \left\| 2\boldsymbol{E} \cdot \boldsymbol{\eta}_E - |\boldsymbol{\eta}_E|^2 \right\| \left\| \xi_{\sigma} \right\| \leq C_{\star} \omega_v^2 \left\| 2\boldsymbol{E} \cdot \boldsymbol{\eta}_E - |\boldsymbol{\eta}_E|^2 \right\|^2 + \frac{1}{8\omega_v^2} \|\xi_{\sigma}\|^2. \tag{A30}$$

Using the regularity assumption on E and Lemma A1, we get

$$\|E \cdot \eta_E\| \le \|E\|_{\infty} \|\eta_E\|, \quad \||\eta_E|^2 \| \le \|\eta_E\|_{\infty} \|\eta_E\| \le C_k \|E\|_{\infty} \|\eta_E\|, \quad (A31)$$

and therefore

$$\left| \left(\mathcal{I}_h \left(2 \boldsymbol{E} \cdot \boldsymbol{\eta}_E - |\boldsymbol{\eta}_E|^2 \right), \xi_\sigma \right) \right| \le C \|\boldsymbol{\eta}_E\|^2 + \frac{1}{8\omega_n^2} \|\xi_\sigma\|^2. \tag{A32}$$

Apply Young's inequality and the approximation properties in Lemma A1, we now bound Λ_3 as

$$\begin{split} |\Lambda_{3}| &\leq \frac{\epsilon_{0} a \theta \gamma_{v}}{2\omega_{v}^{2}} \left(\frac{1}{4} \|\eta_{\sigma}\|^{2} + \|\xi_{\sigma}\|^{2}\right) + \frac{\epsilon_{0} a \theta}{2\omega_{v}^{2}} \left(2\|\partial_{t}\eta_{\sigma} + \omega_{v}^{2}\eta_{Q}\|^{2} + C\|\eta_{E}\|^{2} + \frac{1}{4}\|\xi_{\sigma}\|^{2}\right) \\ &\leq Ch^{2k+2} + \frac{\epsilon_{0} a \theta \gamma_{v}}{2\omega_{v}^{2}} \|\xi_{\sigma}\|^{2} + \frac{\epsilon_{0} a \theta}{8\omega_{v}^{2}} \|\xi_{\sigma}\|^{2}. \end{split} \tag{A33}$$

Step 3.5: to estimate Λ_4 in (A24).

For Λ_4 , using Cauchy Schwartz inequality, Young's inequality, Lemma 1, and Lemma A3, we have

$$\begin{split} |\Lambda_4| &\leq \epsilon_0 \epsilon_\infty \left(\frac{1}{4\alpha_1} \|\partial_t \eta_E\|^2 + \alpha_1 \|\xi_E\|^2\right) + \epsilon_0 \left(\frac{1}{4\alpha_2} \|\eta_J\|^2 + \alpha_2 \|\xi_E\|^2\right) \\ &+ \frac{\epsilon_0 \omega_p^2}{2} \|\mho_E\|^2 + \frac{\epsilon_0}{2\omega_p^2} \|\xi_J\|^2 \\ &+ 3\epsilon_0 a (1-\theta) \|E - \eta_E\|_\infty \|\partial_t (E - \eta_E)\|_\infty \|\xi_E\|^2 + \epsilon_0 a (1-\theta) \\ &\left(\frac{1}{\alpha_3} \int_\Omega \mathcal{I}_h (|\xi_E|^4) d\Omega + \frac{\alpha_3}{4} \|\partial_t (E - \eta_E)\|_\infty^2 \|\xi_E\|^2\right) \\ &+ \epsilon_0 a \theta C_\star \left(\frac{1}{4\alpha_4} \|\partial_t \left(Q\eta_E + \eta_Q (E - \eta_E)\right)\right)^2 + \alpha_4 \|\xi_E\|^2\right) \\ &+ \frac{\epsilon_0 a \theta}{2} \|\partial_t (Q - \eta_Q)\|_\infty \|\xi_E\|^2 \end{split}$$



$$\begin{split} &+ \epsilon_{0} a (1 - \theta) C_{\star} \left(\frac{1}{4\alpha_{5}} \left\| \partial_{t} \left(|\eta_{E}|^{2} \eta_{E} - |\eta_{E}|^{2} E \right) \right. \\ &- 2 (E \cdot \eta_{E}) \eta_{E} + 2 (E \cdot \eta_{E}) E + |E|^{2} \eta_{E} \right) \right\|^{2} + \alpha_{5} \|\xi_{E}\|^{2} \right) \\ &+ \frac{\epsilon_{0} a \theta}{2} \left(\frac{1}{4\alpha_{6}} \|\partial_{t} (E - \eta_{E})\|_{\infty}^{2} \|\xi_{E}\|^{2} + \alpha_{6} \|\xi_{Q}\|^{2} \right), \quad \forall \alpha_{i} > 0, i = 1, \cdots, 6. \end{split}$$

We only choose two terms from Λ_4 to illustrate how the estimation above is obtained,

$$\begin{split} &\left| \int_{\Omega} \mathcal{I}_{h} \left(\partial_{t} (Q - \eta_{Q}) | \boldsymbol{\xi}_{E} |^{2} \right) d\Omega \right| \\ & \leq \left| \sum_{i=1}^{N_{x}} \sum_{j=1}^{N_{y}} \frac{\Delta x_{i}}{2} \frac{\Delta y_{j}}{2} \sum_{m,n=0}^{k} \widehat{\omega}_{m} \widehat{\omega}_{n} \left(\partial_{t} (Q - \eta_{Q}) | \boldsymbol{\xi}_{E} |^{2} \right) (x_{im}, y_{jn}) \right| \\ & \leq \| \partial_{t} (Q - \eta_{Q}) \|_{\infty} \left| \sum_{i=1}^{N_{x}} \sum_{j=1}^{N_{y}} \frac{\Delta x_{i}}{2} \frac{\Delta y_{j}}{2} \sum_{m,n=0}^{k} \widehat{\omega}_{m} \widehat{\omega}_{n} | \boldsymbol{\xi}_{E} |^{2} (x_{im}, y_{jn}) \right| \\ & = \| \partial_{t} (Q - \eta_{Q}) \|_{\infty} \| \boldsymbol{\xi}_{E} \|^{2}, \end{split}$$

and

$$\begin{split} \left| \int_{\Omega} \mathcal{I}_{h} \left(|\boldsymbol{\xi}_{E}|^{2} \partial_{t} (\boldsymbol{E} - \boldsymbol{\eta}_{E}) \cdot \boldsymbol{\xi}_{E} \right) d\Omega \right| & \text{(by Lemmas 1-2)} \\ & \leq \int_{\Omega} \mathcal{I}_{h} \left(|\boldsymbol{\xi}_{E}|^{2} |\partial_{t} (\boldsymbol{E} - \boldsymbol{\eta}_{E})| |\boldsymbol{\xi}_{E}| \right) d\Omega = \int_{\Omega} \mathcal{I}_{h} \left(|\boldsymbol{\xi}_{E}|^{2} \right) \mathcal{I}_{h} \left(|\partial_{t} (\boldsymbol{E} - \boldsymbol{\eta}_{E})| |\boldsymbol{\xi}_{E}| \right) d\Omega \\ & \leq \|\mathcal{I}_{h} \left(|\boldsymbol{\xi}_{E}|^{2} \right) \| \|\mathcal{I}_{h} \left(|\partial_{t} (\boldsymbol{E} - \boldsymbol{\eta}_{E})| |\boldsymbol{\xi}_{E}| \right) \| \\ & \leq \left(\int_{\Omega} \mathcal{I}_{h} (|\boldsymbol{\xi}_{E}|^{4}) d\Omega \right)^{1/2} \|\partial_{t} (\boldsymbol{E} - \boldsymbol{\eta}_{E}) \|_{\infty} \|\boldsymbol{\xi}_{E}\| \\ & \leq \frac{1}{\alpha_{2}} \int_{\Omega} \mathcal{I}_{h} (|\boldsymbol{\xi}_{E}|^{4}) d\Omega + \frac{\alpha_{3}}{4} \|\partial_{t} (\boldsymbol{E} - \boldsymbol{\eta}_{E}) \|_{\infty}^{2} \|\boldsymbol{\xi}_{E}\|^{2}. \end{split}$$

We now specify α_i , $i = 1, \dots, 6$ as follows,

$$\epsilon_0 \epsilon_\infty \alpha_1 = \epsilon_0 \alpha_2 = \epsilon_0 a \theta C_\star \alpha_4 = \epsilon_0 a (1 - \theta) C_\star \alpha_5 = \frac{1}{4} \frac{\epsilon_0 \epsilon_\infty \kappa_{err}}{12}, \quad \alpha_3 = \frac{12}{\rho_{err}}, \quad \alpha_6 = \frac{\rho_{err}}{2}.$$

Moreover we restrict the strength of nonlinearity such that

$$\begin{split} &3\epsilon_0 a(1-\theta) \| \boldsymbol{E} - \boldsymbol{\eta}_{\boldsymbol{E}} \|_{\infty} \| \partial_t (\boldsymbol{E} - \boldsymbol{\eta}_{\boldsymbol{E}}) \|_{\infty} + \left(\epsilon_0 a(1-\theta) \frac{\alpha_3}{4} + \frac{\epsilon_0 a\theta}{8\alpha_6} \right) \| \partial_t (\boldsymbol{E} - \boldsymbol{\eta}_{\boldsymbol{E}}) \|_{\infty}^2 \\ &+ \frac{\epsilon_0 a\theta}{2} \| \partial_t (Q - \eta_Q) \|_{\infty} \leq \frac{\epsilon_0 \epsilon_\infty \kappa_{err}}{4}. \end{split}$$

This can be guaranteed if

$$3a(1-\theta)C_k^2 \|\boldsymbol{E}\|_{\infty} \|\partial_t \boldsymbol{E}\|_{\infty} + (12-11\theta) \frac{aC_k^2}{4\rho_{err}} \|\partial_t \boldsymbol{E}\|_{\infty}^2 + \frac{a\theta}{2} C_k \|\partial_t Q\|_{\infty} \leq \frac{\epsilon_{\infty} \kappa_{err}}{4},$$

holds, which is also Condition 3 in (41). Based on what we have by far, with the approximation properties from Lemma A1, we arrive at



$$|\Lambda_4| \leq CC(\kappa_{err}, \rho_{err})h^{2k+2} + \frac{\epsilon_0 \epsilon_\infty \kappa_{err}}{3} \|\boldsymbol{\xi}_E\|^2 + \frac{\epsilon_0 a(1-\theta)\rho_{err}}{12} \int_{\Omega} \mathcal{I}_h(|\boldsymbol{\xi}_E|^4) d\Omega + \frac{\epsilon_0 a\theta\rho_{err}}{4} \|\boldsymbol{\xi}_Q\|^2 + \frac{\epsilon_0}{2\omega_p^2} \|\boldsymbol{\xi}_J\|^2.$$
(A34)

(2021) 89:45

The combination of (A24)–(A34) gives

$$\frac{d\widehat{\mathcal{E}}_h}{dt} \leq \widehat{\mathcal{E}}_h + CC(\kappa_{err}, \rho_{err})h^{2r},$$

where

$$r = \begin{cases} k, & \text{for central numerical fluxes,} \\ k+1, & \text{for alternating numerical fluxes.} \end{cases}$$

Finally, using Gronwall inequality and $\widehat{\mathcal{E}}_h(0) = 0$, we get $\mathcal{E}_h^{(mod)} \leq \widehat{\mathcal{E}}_h \leq CC(\kappa_{err}, \rho_{err})h^r$. We further apply a triangle inequality and the approximation results in Lemma A1, and conclude

$$||u - u_h|| \le ||\xi_u|| + ||\eta_u|| \le CC(\kappa_{err}, \rho_{err})h^r, \quad u = H_z, E, P, J, \sigma, Q.$$

Appendix B: Proof of Theorem 4

Proof Apply two time steps to (42a) and (42j), sum them up after taking $\phi = H_{zh}^{n+1/2}$, one gets

$$\mu_0 \left(H_{zh}^{n+3/2} - H_{zh}^{n+1/2}, H_{zh}^{n-1/2} \right) + \Delta t \mathcal{B}_h^E (E_{xh}^{n+1} + E_{xh}^n, E_{yh}^{n+1} + E_{yh}^n, H_{zh}^{n+1/2}) = 0.$$
(B1)

Take
$$\phi = E_{xh}^{n+1} + E_{xh}^{n}$$
 in (42b), $\phi = E_{yh}^{n+1} + E_{yh}^{n}$ in (42c), sum them up, we have
$$\left(D_{h}^{n+1} - D_{h}^{n}, E_{h}^{n+1} + E_{h}^{n} \right) + \Delta t \mathcal{B}_{xh}^{H} (H_{zh}^{n+1/2}, E_{xh}^{n+1} + E_{xh}^{n}) + \Delta t \mathcal{B}_{yh}^{H} (H_{zh}^{n+1/2}, E_{yh}^{n+1} + E_{yh}^{n}) = 0.$$
 (B2)

Add (B2) to (B1) and using the identity (30), we obtain

$$\mu_{0} \int_{\Omega} H_{zh}^{n+3/2} H_{zh}^{n+1/2} d\Omega - \mu_{0} \int_{\Omega} H_{zh}^{n+1/2} H_{zh}^{n-1/2} d\Omega + \int_{\Omega} \left(\mathbf{D}_{h}^{n+1} - \mathbf{D}_{h}^{n} \right) \cdot \left(\mathbf{E}_{h}^{n+1} + \mathbf{E}_{h}^{n} \right) d\Omega = 0.$$
 (B3)

By (42d), we have

$$\begin{split} & \int_{\Omega} \left(\boldsymbol{D}_{h}^{n+1} - \boldsymbol{D}_{h}^{n} \right) \cdot \left(\boldsymbol{E}_{h}^{n+1} + \boldsymbol{E}_{h}^{n} \right) d\Omega \\ & = \epsilon_{0} \epsilon_{\infty} \int_{\Omega} |\boldsymbol{E}_{h}^{n+1}|^{2} d\Omega - \epsilon_{0} \epsilon_{\infty} \int_{\Omega} |\boldsymbol{E}_{h}^{n}|^{2} d\Omega + \epsilon_{0} \int_{\Omega} \left(\boldsymbol{P}_{h}^{n+1} - \boldsymbol{P}_{h}^{n} \right) \cdot \left(\boldsymbol{E}_{h}^{n+1} + \boldsymbol{E}_{h}^{n} \right) d\Omega \end{split}$$



Page 40 of 42

$$+ \epsilon_{0} a(1 - \theta) \int_{\Omega} \left(\boldsymbol{Y}_{h}^{n+1} - \boldsymbol{Y}_{h}^{n} \right) \cdot \left(\boldsymbol{E}_{h}^{n+1} + \boldsymbol{E}_{h}^{n} \right) d\Omega$$

$$+ \epsilon_{0} a\theta \int_{\Omega} \left(\mathcal{I}_{h} \left(\boldsymbol{Q}_{h}^{n+1} \boldsymbol{E}_{h}^{n+1} \right) - \mathcal{I}_{h} \left(\boldsymbol{Q}_{h}^{n} \boldsymbol{E}_{h}^{n} \right) \right) \cdot \left(\boldsymbol{E}_{h}^{n+1} + \boldsymbol{E}_{h}^{n} \right) d\Omega.$$
(B4)

For the nonlinear Kerr term, by (42e) and Lemma 1, we get

$$\int_{\Omega} \left(Y_{h}^{n+1} - Y_{h}^{n} \right) \cdot \left(E_{h}^{n+1} + E_{h}^{n} \right) d\Omega
= \int_{\Omega} \mathcal{I}_{h} \left(\left(|E^{n+1}|^{2} + |E^{n}|^{2} - E^{n+1} \cdot E^{n} \right) \left(E^{n+1} - E^{n} \right) \right) \cdot \left(E_{h}^{n+1} + E_{h}^{n} \right) d\Omega
+ \frac{1}{2} \int_{\Omega} \mathcal{I}_{h} \left((E^{n+1} + E^{n}) \cdot (E^{n+1} - E^{n})(E^{n+1} + E^{n}) \right) \cdot \left(E_{h}^{n+1} + E_{h}^{n} \right) d\Omega
= \frac{1}{2} \int_{\Omega} \mathcal{I}_{h} \left(\left(2|E^{n+1}|^{2} + 2|E^{n}|^{2} - 2E^{n+1} \cdot E^{n} + |E_{h}^{n+1} + E_{h}^{n}|^{2} \right) \left(|E^{n+1}|^{2} - |E^{n}|^{2} \right) \right) d\Omega
= \frac{3}{2} \int_{\Omega} \mathcal{I}_{h} \left(|E^{n+1}|^{4} \right) d\Omega - \frac{3}{2} \int_{\Omega} \mathcal{I}_{h} \left(|E^{n}|^{4} \right) d\Omega.$$
(B5)

For the Lorentz term, using (42f) and (42g), we have

$$\begin{split} &\int_{\Omega} \left(\boldsymbol{P}_{h}^{n+1} - \boldsymbol{P}_{h}^{n} \right) \cdot \left(\boldsymbol{E}_{h}^{n+1} + \boldsymbol{E}_{h}^{n} \right) d\Omega \\ &= \frac{2}{\omega_{p}^{2}} \int_{\Omega} \left(\boldsymbol{P}_{h}^{n+1} - \boldsymbol{P}_{h}^{n} \right) \cdot \left(\frac{\boldsymbol{J}_{h}^{n+1} - \boldsymbol{J}_{h}^{n}}{\Delta t} + \gamma \frac{\boldsymbol{J}_{h}^{n+1} + \boldsymbol{J}_{h}^{n}}{2} + \omega_{0}^{2} \frac{\boldsymbol{P}_{h}^{n+1} + \boldsymbol{P}_{h}^{n}}{2} \right) d\Omega \\ &= \frac{1}{\omega_{p}^{2}} \int_{\Omega} |\boldsymbol{J}_{h}^{n+1}|^{2} d\Omega - \frac{1}{\omega_{p}^{2}} \int_{\Omega} |\boldsymbol{J}_{h}^{n}|^{2} d\Omega + \frac{\gamma \Delta t}{2\omega_{p}^{2}} \int_{\Omega} |\boldsymbol{J}_{h}^{n+1} + \boldsymbol{J}_{h}^{n}|^{2} d\Omega \\ &+ \frac{\omega_{0}^{2}}{\omega_{p}^{2}} \int_{\Omega} |\boldsymbol{P}_{h}^{n+1}|^{2} d\Omega - \frac{\omega_{0}^{2}}{\omega_{p}^{2}} \int_{\Omega} |\boldsymbol{P}_{h}^{n}|^{2} d\Omega. \end{split} \tag{B6}$$

For the nonlinear Raman term, we have

$$\int_{\Omega} \left(\mathcal{I}_{h} \left(Q_{h}^{n+1} \boldsymbol{E}_{h}^{n+1} \right) - \mathcal{I}_{h} \left(Q_{h}^{n} \boldsymbol{E}_{h}^{n} \right) \right) \cdot \left(\boldsymbol{E}_{h}^{n+1} + \boldsymbol{E}_{h}^{n} \right) d\Omega
= \int_{\Omega} \mathcal{I}_{h} \left(Q_{h}^{n+1} |\boldsymbol{E}_{h}^{n+1}|^{2} \right) d\Omega - \int_{\Omega} \mathcal{I}_{h} \left(Q_{h}^{n} |\boldsymbol{E}_{h}^{n}|^{2} \right) d\Omega
+ \int_{\Omega} \left(Q_{h}^{n+1} - Q_{h}^{n} \right) \mathcal{I}_{h} \left(\boldsymbol{E}_{h}^{n+1} \cdot \boldsymbol{E}_{h}^{n} \right) d\Omega, \tag{B7}$$

where the last term can be further proceeded based on (42h) and (42i),

$$\begin{split} &\int_{\Omega} (Q_h^{n+1} - Q_h^n) \mathcal{I}_h \left(E_h^{n+1} \cdot E_h^n \right) d\Omega \\ &= \frac{1}{\omega_v^2} \int_{\Omega} (Q_h^{n+1} - Q_h^n) \left(\frac{\sigma_h^{n+1} - \sigma_h^n}{\Delta t} + \gamma_v \frac{\sigma_h^{n+1} + \sigma_h^n}{2} + \omega_v^2 \frac{Q_h^{n+1} + Q_h^n}{2} \right) d\Omega \\ &= \frac{1}{2\omega_v^2} \int_{\Omega} (\sigma_h^{n+1})^2 d\Omega - \frac{1}{2\omega_v^2} \int_{\Omega} (\sigma_h^n)^2 d\Omega \\ &+ \frac{\gamma_v \Delta t}{4\omega_v^2} \int_{\Omega} (\sigma_h^{n+1} + \sigma_h^n)^2 d\Omega + \frac{1}{2} \int_{\Omega} (Q_h^{n+1})^2 d\Omega - \frac{1}{2} \int_{\Omega} (Q_h^n)^2 d\Omega. \end{split} \tag{B8}$$

Combine (B3)–(B8), we reach the energy relation (43) with the discrete energy \mathcal{E}_h^n defined in (44).



The next step is to derive the time step condition under which the discrete energy \mathcal{E}_h^n is nonnegative. Based on (42a) and (42j), we have

$$\mu_{0}\left(H_{zh}^{n+1/2} - H_{zh}^{n-1/2}, \phi\right) - \Delta t \sum_{i=1}^{N_{x}} \int_{y_{a}}^{y_{b}} \widehat{E_{yh}^{n}}[\phi]_{x_{i+\frac{1}{2}}} dy + \Delta t \sum_{j=1}^{N_{y}} \int_{x_{a}}^{x_{b}} \widehat{E_{xh}^{n}}[\phi]_{y_{j+\frac{1}{2}}} dx - \Delta t(E_{yh}^{n}, \partial_{x}\phi) + \Delta t(E_{xh}^{n}, \partial_{y}\phi) = 0.$$
(B9)

Take $\phi = H_{7h}^{n+1/2}$, using the inverse inequality (A5), we obtain

(2021) 89:45

$$\begin{split} &\mu_{0} \int_{\Omega} \left(H_{zh}^{n+1/2}\right)^{2} d\Omega - \mu_{0} \int_{\Omega} H_{zh}^{n+1/2} H_{zh}^{n-1/2} d\Omega \\ &= \Delta t \sum_{i=1}^{N_{x}} \int_{y_{a}}^{y_{b}} \widehat{E_{yh}^{n}} \left[H_{zh}^{n+1/2}\right]_{x_{i+\frac{1}{2}}} dy - \Delta t \sum_{j=1}^{N_{y}} \int_{x_{a}}^{x_{b}} \widehat{\widehat{E_{xh}^{n}}} \left[H_{zh}^{n+1/2}\right]_{y_{j+\frac{1}{2}}} dx \\ &+ \Delta t (E_{yh}^{n}, \partial_{x} H_{zh}^{n+1/2}) - \Delta t (E_{xh}^{n}, \partial_{y} H_{zh}^{n+1/2}) \\ &\leq \frac{\Delta t C_{\star}}{h} \left(\int_{\Omega} \left|E_{h}^{n}\right|^{2} d\Omega + \int_{\Omega} \left(H_{zh}^{n+1/2}\right)^{2} d\Omega \right), \end{split} \tag{B10}$$

hence,

$$\frac{\mu_0}{2} \int_{\Omega} H_{zh}^{n+1/2} H_{zh}^{n-1/2} d\Omega \geq \left(\frac{\mu_0}{2} - \frac{\Delta t C_{\star}}{2h}\right) \int_{\Omega} \left(H_{zh}^{n+1/2}\right)^2 d\Omega - \frac{\Delta t C_{\star}}{2h} \int_{\Omega} \left|E_h^n\right|^2 d\Omega.$$

This implies, if we restrict the time step Δt such that,

$$\frac{\mu_0}{2} - \frac{\Delta t C_{\star}}{2h} \ge 0, \quad \frac{\epsilon_0 \epsilon_{\infty}}{2} - \frac{\Delta t C_{\star}}{2h} \ge 0,$$

then by Lemma 1 and with the condition $\theta \in [0, \frac{3}{4}]$, we have

$$\mathcal{E}_{h}^{n} \geq \int_{\Omega} \frac{\epsilon_{0} a \theta}{4} \mathcal{I}_{h} \left(\left(\left| \boldsymbol{E}_{h}^{n} \right|^{2} + \left(\boldsymbol{Q}_{h}^{n} \right)^{2} \right)^{2} \right) + \frac{\epsilon_{0} a (3 - 4 \theta)}{4} \mathcal{I}_{h} \left(\left| \boldsymbol{E}_{h}^{n} \right|^{4} \right) d\Omega \geq 0.$$

References

- Anees, A., Angermann, L.: Energy-stable time-domain finite element methods for the 3D nonlinear Maxwell's equations. IEEE Photonics J. 12(2), 1–15 (2020)
- Appelö, D., Bokil, V.A., Cheng, Y., Li, F.: Energy stable SBP-FDTD methods for Maxwell-Duffing models in nonlinear photonics. IEEE J. Multiscale Multiphys. Comput. Tech. 4, 329–336 (2019)
- Bokil, V.A., Cheng, Y., Jiang, Y., Li, F.: Energy stable discontinuous Galerkin methods for Maxwell's equations in nonlinear optical media. J. Comput. Phys. 350, 420–452 (2017)
- Bokil, V.A., Cheng, Y., Jiang, Y., Li, F., Sakkaplangkul, P.: High spatial order energy stable FDTD methods for Maxwell's equations in nonlinear optical media in one dimension. J. Sci. Comput. 77(1), 330–371 (2018)
- Bokil, V.A., Gibson, N.L., Gyrya, V., McGregor, D.A.: Dispersion reducing methods for edge discretizations of the electric vector wave equation. J. Comput. Phys. 287, 88–109 (2015)
- 6. Boyd, R.W.: Nonlinear Optics. Academic Press, New York (2003)
- 7. Chen, C.-L.: Optical Solitons in Optical Fibers. Wiley, New York (2005)
- Ciarlet, P.G.: Finite Element Method for Elliptic Problems. Society for Industrial and Applied Mathematics, Philadelphia (2002)



- Cockburn, B., Kanschat, G., Perugia, I., Schötzau, D.: Superconvergence of the local discontinuous Galerkin method for elliptic problems on Cartesian grids. SIAM J. Numer. Anal. 39(1), 264–285 (2001)
- Cockburn, B., Singler, J.R., Zhang, Y.: Interpolatory HDG method for parabolic semilinear PDEs. J. Sci. Comput. 79(3), 1777–1800 (2019)
- Fezoui, L., Lanteri, S.: Discontinuous Galerkin methods for the numerical solution of the nonlinear Maxwell equations in 1d. Ph.D. thesis, Inria (2015)
- Fisher, A., White, D., Rodrigue, G.: An efficient vector finite element method for nonlinear electromagnetic modeling. J. Comput. Phys. 225(2), 1331–1346 (2007)
- Gilles, L., Hagness, S.C., Vázquez, L.: Comparison between staggered and unstaggered finite-difference time-domain grids for few-cycle temporal optical soliton propagation. J. Comput. Phys. 161(2), 379–400 (2000)
- Greene, J., Taflove, A.: Scattering of spatial optical solitons by subwavelength air holes. IEEE Microwave Wirel. Compon. Lett. 17, 760–762 (2007)
- Greene, J.H., Taflove, A.: General vector auxiliary differential equation finite-difference time-domain method for nonlinear optics. Opt. Express 14(18), 8305–8310 (2006)
- Hesthaven, J.S., Warburton, T.: Nodal Discontinuous Galerkin Methods: Algorithms, Analysis, and Applications. Springer, Berlin (2007)
- 17. Huang, J., Shu, C.-W.: A second-order asymptotic-preserving and positivity-preserving discontinuous Galerkin scheme for the Kerr-Debye model. Math. Models Methods Appl. Sci. 27(03), 549–579 (2017)
- 18. Jackson, J.D.: Classical Electrodynamics. Wiley, New York (1999)
- Jia, H., Li, J., Fang, Z., Li, M.: A new FDTD scheme for Maxwell's equations in Kerr-type nonlinear media. Numer. Algorithms 82, 223–243 (2019)
- Li, J., Shi, C., Shu, C.W.: Optimal non-dissipative discontinuous Galerkin methods for Maxwell's equations in Drude metamaterials. Comput. Math. Appl. 73(8), 1760–1780 (2017)
- 21. Pantell, R.H., Puthoff, H.E.: Fundamentals of Quantum Electronics. Wiley, New York (1969)
- Peng, Z., Bokil, V.A., Cheng, Y., Li, F.: Asymptotic and positivity preserving methods for Kerr–Debye model with Lorentz dispersion in one dimension. J. Comput. Phys. 402, 109101 (2019)
- Xing, Y., Chou, C.S., Shu, C.W.: Energy conserving local discontinuous Galerkin methods for wave propagation problems. Inverse Probl. Imaging 7(3), 967–986 (2013)

Publisher's Note Springer Nature remains neutral with regard to jurisdictional claims in published maps and institutional affiliations.

